Leona Otega Ojake
BSc Biology

Novel Biohybrid Systems for the Production of Solar Fuels

Dissertation to obtain the Master's Degree in Biotechnology for Sustainability

April/2022

Supervisor: Dr. Mónica Martins Neves, Senior Researcher in Bacterial Energy Metabolism laboratory (ITQB NOVA)

Co-Supervisor: Prof. Inês Cardoso Pereira, Principal Investigator in Bacterial Energy Metabolism laboratory (ITQB NOVA)

Leona Otega Ojake
BSc Biology

Novel Biohybrid Systems for the Production of Solar Fuels

Dissertation to obtain the Master's Degree in Biotechnology for Sustainability

April/2022

Supervisor: Dr. Mónica Martins Neves, Senior Researcher in Bacterial Energy Metabolism laboratory (ITQB NOVA)

Co-Supervisor: Prof. Inês Cardoso Pereira, Principal Investigator in Bacterial Energy Metabolism laboratory (ITQB NOVA)

Jury:
President:
Opponent:

Novel biohybrid systems for the production of solar fuels

Acknowledgements

This dissertation would not have been possible without the support, guidance and help from my supervisors Dr. Mónica Martins Neves and Prof. Inês Cardoso Pereira of the Bacterial Energy Metabolism (BEM) laboratory at ITQB. Thank you for all you have taught me and your continuous support. Many thanks equally to the other members of the BEM laboratory for their advice, moral support, and for lending a helping hand on more than one occasion. Thank you Américo Duarte, Ana Barbosa, Ana Margarida Coito, Ana Rita Oliveira, Adreia Pimenta, Diogo Grilo, Gonçalo Manteigas and Rita Manuel. Thank you to the coordinators and all teaching staff of the Master's course in Biotechnology for Sustainability who have given me the tools needed to make it to this point. I would also like to thank my family and friends; without their support I would not be here today.

Resumo

O aumento insustentável da emissão de gases com efeito de estufa do sector energético está a aumentar a procura de combustíveis limpos e de produção sustentável para fechar o ciclo antropogénico do carbono. A luz solar fornece mais energia num dia do que a humanidade necessita num ano, a conversão da mesma em combustíveis é uma área que tem vindo a crescer de forma significativa e é altamente promissora.

Os sistemas fotossintéticos bio-híbridos, acoplando catalisadores de células inteiras com semicondutores produzidos por microrganismos não fotossintéticos auto-fotosensibilizados, surgiram como uma abordagem potencial para a produção de combustíveis solares num processo conhecido como fotossíntese semi-artificial. O objectivo desta tese é a criação de novos sistemas bio-híbridos utilizando os microrganismos *Desulfovibrio desulfuricans* e *Desulfovibrio vulgaris* Hildenborough para a conversão leve de CO_2 em compostos de valor acrescentado e para a produção sustentável de combustível hidrogénio (H_2).

O desempenho dos sistemas bio-híbridos foi igualmente avaliado na presença de diferentes co-catalisadores, nomeadamente molibdénio (Mo) e nanopartículas biogénicas de platina (BioPt) e paládio (BioPd). O sistema bio-híbrido optimizado foi capaz de catalisar a produção de 149 ± 8 µmol de H_2 após uma produção contínua ao longo de 141 horas. A redução bem-sucedida de CO_2 no formato composto de armazenamento de hidrogénio foi conseguida, com um sistema bio-híbrido construído utilizando uma estirpe recombinante de *D. vulgaris* com níveis de expressão aumentados do formato desidrogenase FdhAB capaz de produzir 18 ± 1 mM de formato na presença de um vaivém de electrões. Finalmente, foi montado com sucesso um reator à escala de bancada para a produção de Hidrogénio leve, levando à produção de 10 ± 1mM de H_2. Os resultados obtidos nesta tese mostram, portanto que tanto *D. desulfuricans* como *D. vulgaris* Hildenborough são candidatos promissores para a utilização da produção de combustível fotocatalítico em fotossíntese semi-artificial.

Palavras-chave: hidrogénio, combustível solar, sistema bio-híbrido, fotocatálise, fotossíntese semi-artificial

Abstract

Greenhouse gas emissions from the energy sector being one of the major contributors to climate change, the search for clean sustainable fuels and a sustainable means to close the anthropogenic carbon cycle are more pressing than ever. Sunlight provides more energy in a day than humanity requires in a year, thus the conversion of solar energy into fuels is an expanding and highly promising area.

Biohybrid photosynthetic systems, coupling whole cell catalysts with semiconductors produced by self-photosensitised non-photosynthetic microorganisms, have emerged as a potential approach for the production of solar fuels in a process known as semi-artificial photosynthesis. The objective of the following work is the creation of novel biohybrid systems using different combinations of microorganisms and semiconductors for the light driven conversion of CO_2 into value-added compounds and the sustainable production of hydrogen (H_2) fuel.

Among the different biohybrid systems created, the most efficient biohybrid system constructed of *Desulfovibrio* with 3 mM of cadmium sulfide (CdS) as a semiconductor, 0.1 mM molybdenum and 2ml biogenic palladium nanoparticles as co-catalysts was able to catalyse the production of 149 ± 8 µmol of H_2 after continuous production over 141 hours, reaching an AQY of 23% in the absence of an electron shuttle. Concerning CO_2 reduction, its successful reduction into the hydrogen storage compound formate was achieved, with a biohybrid system constructed using a recombinant strain of *D. vulgaris* Hildenborough with increased expression levels of the formate dehydrogenase FdhAB able to produce 18 ± 1 mM of formate. Finally, a bench-scale reactor was successfully set up for the light-driven production of Hydrogen, leading to the production of 10 ± 1 mM of H_2. The results obtained in this thesis therefore show that biohybrids produced with *D. desulfuricans* and *D. vulgaris* Hildenborough are promising candidates for photocatalytic fuel production in semi-artificial photosynthesis.

Keywords: hydrogen, solar fuel, biohybrid system, photocatalysis, semi-artificial photosynthesis

Table of Contents

List of Figures

List of Tables

Abbreviations

$AgInS_2$ – silver indium sulfide

AQY – apparent quantum yield

AuNC – gold nanocluster

BioPd – biogenic palladium nanoparticle

BioPt – biogenic platinum nanoparticle

CCS – carbon capture and storage

CCU – carbon capture and utilisation

Cd – cadmium

CD – carbon dot

CdS – cadmium sulfide

CH_4 – methane

C_2H_4 - ethylene

CO – carbon monoxide

CO_2 – carbon dioxide

Cr – chromium

$CuInS_2$ – copper indium sulfide

EDS – energy dispersive spectrometry

FDH – formate dehydrogenase

Fe – iron

GC – gas chromatography

g_{dcw} – gram dry cell weight

H_2 – molecular hydrogen

H_2S – hydrogen sulfide

HPLC – high performance liquid chromatography

IEA – international energy agency

In_2S_3 – indium(III) sulfide

LED – light emitting diode

Mo – molybdenum

MoS_2 – molybdenum disulfide

MV – methyl viologen

N_2 – molecular nitrogen

NH_3 – ammonia

Ni – nickel

NP – nanoparticle

OD_{600} – optical density at 600 nm

Pd – palladium

PdS – palladium sulfide

PPBS – periplasmic photosensitised biohybrid system

Pt – platinum

QD – quantum dot

QE – quantum efficiency

S – sulfur

Se – selenium

SED – sacrificial electron donor

SEM – scanning electron microscopy

TEM – transmission electron microscopy

TiO_2 – titanium dioxide

W – tungsten

WLP – Wood-Ljungdahl pathway

XRD – x-ray diffraction

Zn – zinc

1 Introduction

Over the span of the last century or more, human development, particularly in the industrialised nations of the western world, was inextricably linked to the use of fossil fuels, creating an interdependence between the two. Most major inventions are tied to fossil fuels, such as the invention of the car, electricity, and, most recently, the internet. Whilst many technological advancements that we have seen would not have been possible without the utilisation of fossil fuels, the use thereof invariably brought along with it major drawbacks, at the forefront of which high levels of environmental pollution associated both with the sourcing as well as burning of fossil fuels (1).

However, global energy demand is only expected to rise continually in the future, resulting from projected growth in industry, economy as well as population all over the world (2). In 2018, the three biggest energy sources used worldwide were oil (31.6%), coal (26.9%) and natural gas (22.8%), all of which are carbon-based and vastly contribute to the emission of greenhouse gases resulting in global warming and climate change. Of the carbon dioxide (CO_2) emissions released from the energy sector alone, more than 99% is attributed to these three sources of fossil fuels (3).

A shift away from the reliance on fossil fuels is therefore increasingly necessary, and while difficult, it is not impossible. Despite the transition into renewable energy being hindered by those heavily invested in the fossil fuel sector, a few green energy sources have been implemented on an ever growing scale for the past few decades, such as wind, solar, hydropower or geothermal, marking the beginning of a much needed change (4).

1.1 The anthropogenic CO_2 cycle

Fossil CO_2 dominates the anthropogenic greenhouse gas emissions responsible for driving climate change (reviewed in (5)). The BP Statistical Review of World Energy 2020 states that global CO_2 emissions due to the consumption of fossil fuels such as oil, coal and gas in 2019 was at 34,169 billion tons (6). To put this into historic context, the emissions in 2019 represented an increase of 60.1% compared to those in 1990, and a minimum of 40% when compared to the year 2000 (reviewed in (5)). Targets by the European Union to reach climate neutrality by 2050 (7) as well as the ambitious goal of the Paris climate agreement to limit global warming to an 1.5°C increase compared to pre-industrial levels (8) will be paramount in the circumvention of disaster and the averting of the worsening of climate change.

Although the expansion of fossil-fuel based energy infrastructure might be slowing (9), it is by no means close to being halted. With so much CO_2 already in the atmosphere and much more to be accumulated

through ongoing energy infrastructure projects reliant on fossil fuels (10), reducing emissions is no longer sufficient and reaching a safe climate environment is reliant on so-called "negative emissions". Whilst tree planting provides valuable benefits to natural carbon sequestration as well as improving human well-being, it is no longer sufficient to mitigate the continuous increase of CO_2 emissions into the atmosphere, and further strategies for the reduction and removal of greenhouse gas emissions are necessary (11,12). In order to achieve this, two main strategies will require intensive innovation and development as soon as possible in order for their large-scale adoption and application. One of these techniques is carbon capture and storage (CCS), in which anthropogenic CO_2 is captured from emission sources, transported to suitable storage sites such as underground geological formations, and subsequently buried (13). Taking this one step further into the direction of a circular economy is a process called carbon capture and utilisation (CCU), in which the captured carbon is used as a resource itself for subsequent conversion into value-added products or services (14).

1.2 Solar fuels

In addition to the closing of the anthropogenic CO_2 cycle, the expansion of existing alternative and renewable energy sources plays a major role. One of the more established alternative energies is the conversion of sunlight, a free and virtually inexhaustible resource that is democratically available to everyone. The energy provided by sunlight is the most sustainable energy source available. Providing approximately 120,000 TW of energy, solar energy far exceeds the earths global annual energy consumption of approximately 15 TW, and does so in a completely free and, most importantly, non-polluting manner (15–17).

To date, the most widespread applications for the conversion of sunlight into a more accessible form of energy are reliant on photovoltaics (18,19), which are still far from providing the efficient solar-to-energy conversions needed (20). The conversion of solar energy into electricity by photovoltaic and electrochemical solar cells at present is able to reach an efficiency of up to 55-77% (21–24). However, factors such as the high cost of equipment fabrication, inefficient light absorption (25) and low efficiencies in the charge transfer (21) contribute to these technologies remaining uneconomical and limiting their potential for wide-spread application.

The process of converting solar energy into fuels, known as artificial photosynthesis, circumvents the drawbacks seen in photovoltaics (namely its problems with energy storage, intermittency, as well as electricity transmission over long distances), through the storage of solar energy in chemical bonds rather than batteries, relying on synthetic light absorbers and catalysts (20). One of these possible solar fuels gaining more attention is the conversion of sunlight into hydrogen (26). The idea of implementing

solutions for hydrogen to play a substantial part in the transition towards a more sustainable future is not a new one and has received strong support as early as the beginning of the 21st century by both the scientific community as well as the International Energy Agency (IEA) (27).

Molecular hydrogen (H_2) has gained a lot of attention as an attractive energy source, due to an inert high energy content and a complete absence of a negative contribution to the greenhouse effect and therefore global warming when burned. At present however, the use of H_2 as a viable and sustainable fuel alternative is far from efficient. Current means of H_2 production are reliant on fossil fuels and therefore continue to feed into the cycle of greenhouse gas emissions and environmental harm (28). Producing H_2 from sustainable and renewable resources is therefore fundamentally important to achieving viability as a fossil fuel alternative.

1.3 Light-driven H_2 production and CO_2 reduction

The catalytic conversion of light energy into fuels or chemicals is called photocatalysis. Simply defined, the term photocatalysis describes the change in the reaction rate of a catalyst in response to the absorbance of light (29). Photocatalytic reactions using semiconductors for the production of H_2 fuel and the reduction of CO_2 provide interesting angles in the search for clean and sustainable energy. These processes can be of chemical or biological origin.

1.3.1 Chemical processes for the light-driven production of H_2 and light-driven reduction of CO_2

Photocatalytic water splitting, the process in which water is split into H_2 and oxygen (O_2), is gaining more and more attention. With the use of semiconductors, the technology has the potential to provide clean H_2 fuel, as water splitting does not produce any emissions (28).

Successfully constructed systems based on photocatalysts of Pt/CdS (30), Pt-PdS/CdS (31) as well as Zn/Cr layered double hydroxide (32) have demonstrated promising results in the production of H_2 and oxygen through water splitting by visible light, however overall quantum efficiencies are still far below the designated initial starting point (approximately 30% at 600 nm) to allow for practical applications (33,34).

The potential of the TiO_2 semiconductor for photocatalytic water splitting was first demonstrated by Fujishima and Honda in 1972, triggering the development of a research field assessing the use of

photocatalytic semiconductor activity across a variety of applications spanning energy and environment (35,36).

To date, a variety of photocatalysts have been successfully used and shown high quantum efficiencies for the production of H_2 from water splitting under irradiation with UV (reviewed in (37)).

The photocatalytic splitting of water into H_2 and O_2 with the use of semiconductors is a three-step process (Fig. 1.1) (38,39) :

1) The absorption of photons; energies need to exceed the bandgap of the semiconductor, therefore creating an electron (e^-) and hole (h^+) pair
2) The separation of charges and migration of photoexcited charge carriers in the semiconductor
3) Chemical reactions at the semiconductor surface between the charge carriers and reagent compounds (H_2O); alternatively, a recombination of the e^- and h^+ without any chemical reaction happening

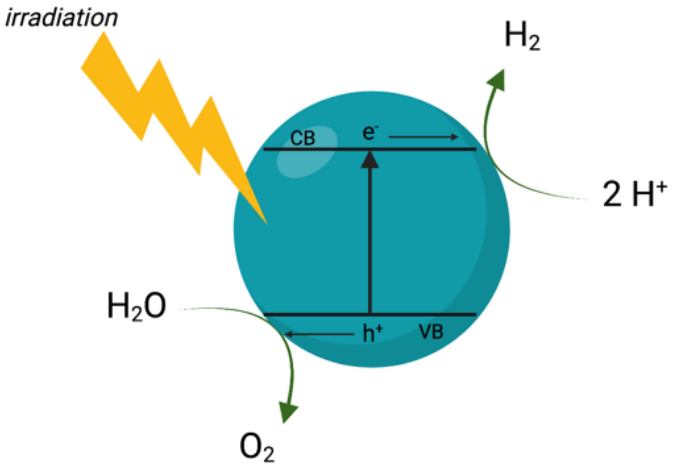

***Figure 1.1**: The water splitting reaction on a semiconductor. Created with BioRender.com*

Pioneered in 1979 by Inoue et al. (40), the photocatalytic reduction of CO_2 is an important step towards the closing of the carbon cycle, however due to poor product selectivity and activity of the semiconductors used in this process remains far from achieving the necessary efficiencies (41). As the highest carbon oxidation state, CO_2 reduction can lead to the production of a variety of C1 as well as C2 products such as carbon monoxide (CO), methane (CH_4) or ethylene (C_2H_4) (reviewed in (41)).

Similarly, to the water splitting reaction, photocatalytic CO_2 reduction occurs in a three step process (42):

1) Light absorption
2) Charge separation and migration
3) Catalytic reduction of CO_2 and oxidation of H_2O

With only ~ 4% of the solar spectrum falling within the UV region and visible light making up ~ 46%, a major drawback of oxide photocatalysts lies in them showing activity only under irradiation with UV. Whilst different approaches have been tested to allow for water splitting activity under visible light irradiation, the search for stable and efficient photocatalysts active under visible light is paramount in order to allow for economically feasible large-scale solar fuel production (39).

1.3.2 Biological processes for the light-driven production of H_2

Whilst green H_2 production can be achieved via the use of the two currently most prominent renewable energies, wind and solar, another production method has received increased interest recently, namely biological hydrogen production. The so-called biohydrogen that is being produced is a result of the catalytic activity of microorganisms, involving two possible groups of enzymes, namely hydrogenases and nitrogenases, with the former being the most important ones (43). Hydrogenases are found across bacteria and archaea, particularly within the genome of anaerobic bacteria (44) as well as lower eukaryotes and fulfil a range of different redox and signalling purposes in their native microorganisms. The oxidation of H_2, as well as the reduction of protons – its reverse reaction- are important for energy capture, for the modulation of an organisms energy input / output, for the adjustment of organelle redox potential, and for the transduction of chemical signals (45)(46)(47). The physiological role of hydrogenases in prokaryotes is very diverse, H_2 being for example a terminal product in many fermentation processes of anaerobic microorganisms. H_2 oxidation is however not limited to anaerobic microorganisms, and H_2 is used widely as an energy source by both aerobic as well as anaerobic microorganisms (48).

Microbial H_2 production can occur via a range of different processes, namely direct and indirect biophotolysis, a microbial water-gas shift, and fermentation processes (photofermentation and dark fermentation) (49).

The process of direct biophotolysis is attractive for the production of sustainable biohydrogen as solar energy is directly used for water splitting (49). For example, low-light intensity *in vivo* assays with *Chlamydomonas reinhardtii* reported a high conversion efficiency of 22% from solar energy to

molecular H_2, however limitations remain due to the [Fe]-hydrogenase present in this organism being highly sensitive to the presence of oxygen. The maintenance of the low oxygen pressure necessary in practice however is practically close to impossible, as the removal of the generated oxygen from the reaction itself would be reliant on huge amounts of carrier gas and is an energy costly process (50).

Indirect biophotolysis is a two-step process in which the production of carbohydrates from photosynthesis is subjected to a following fermentation step for the production of H_2. Both reactions occur with a temporal and / or spatial separation within the microbial cell, allowing for separate evolution of both O_2 and H_2 (51). Indirect biophotolytic abilities have been found in algae and certain species of cyanobacteria (49).

The microbial water-gas shift reaction has been identified in some thermophilic and mesophilic microbial species and results in the production of H_2 and CO_2 (49). In the process, a monofunctional [NiFe]-carbon monoxide dehydrogenase oxidises CO, and an energy-conserving [NiFe]-hydrogenase subsequently catalyses the reduction of protons using the released electrons for the production of molecular H_2 (52). This process, however, remains in the laboratory due to intrinsic limitations such as problems arising from the gaseous nature of the feedstock as well as the inherent toxicity of CO to the biocatalysts (53).

In the process of photofermentative H_2 production, a variety of organic substrates under anaerobic conditions and illumination are oxidised and lead to the generation of H_2 and CO_2 (54). In organisms undergoing photofermentative H_2 production, nitrogenases catalyse the evolution of molecular H_2 under nitrogen-deficient conditions using the energy provided by light and reduced compounds as electron donors (55). Photofermentation has been observed in both phototrophic prokaryotes and eukaryotes, such as green and purple sulfur bacteria, non-sulfur bacteria (56) as well as certain species of green algae (57).

Possibly the most widely studied H_2 production process in microbes is dark fermentation, in which strict or facultative anaerobic bacteria produce H_2 under anaerobic conditions using a variety of organic compounds such as lipids, carbohydrates or proteins as substrates (49).

1.3.3 Biological processes for the light-driven reduction of CO_2

Historically, it was believed that primary organic production, i. e. direct organic synthesis from CO_2, was solely found in plants. Carbon fixation in plants occurs via the Calvin-Benson-Bassham (CBB) cycle, and photosynthesis had been thought to be unequivocally linked to this cycle (58). However, through the use of microbiology techniques it became clear that many microorganisms are also capable of performing photosynthesis, suggesting that it evolved initially in prokaryotes rather than plants (59). Indeed, prokaryotes have evolved a variety of metabolic pathways for the fixation of inorganic carbon

into organic carbon. To date, five pathways in addition to the CBB cycle have been described; the reductive tricarbocyclic acid cycle, the Wood-Ljungdahl pathway (WLP), the 3-Hydroxypropionate4-hydroxybutyrate cycle, the Dicarboxylate4-hydroxybutyrate cycle and the 3-Hydroxypropionate bi-cycle (60).

In the WLP, CO_2 is converted by autotrophic and anaerobic microorganisms into acetic acid, and subsequently reduced into acetyl-CoA (Fig. 1.2) (61). Found among the phyla of proteobacteria, spirochaetes, planctomyces and euryarchaeota, H_2 is used in the WLP as an electron donor, driving the biosynthesis of organic compounds through the simultaneous reduction and oxidation of the electron acceptor CO_2 (62).

Carbon fixation under the WLP occurs via enzymatic reduction to acetyl-CoA, which is then further used for the biosynthesis of proteins or undergoes oxidation to acetate and ATP (63).

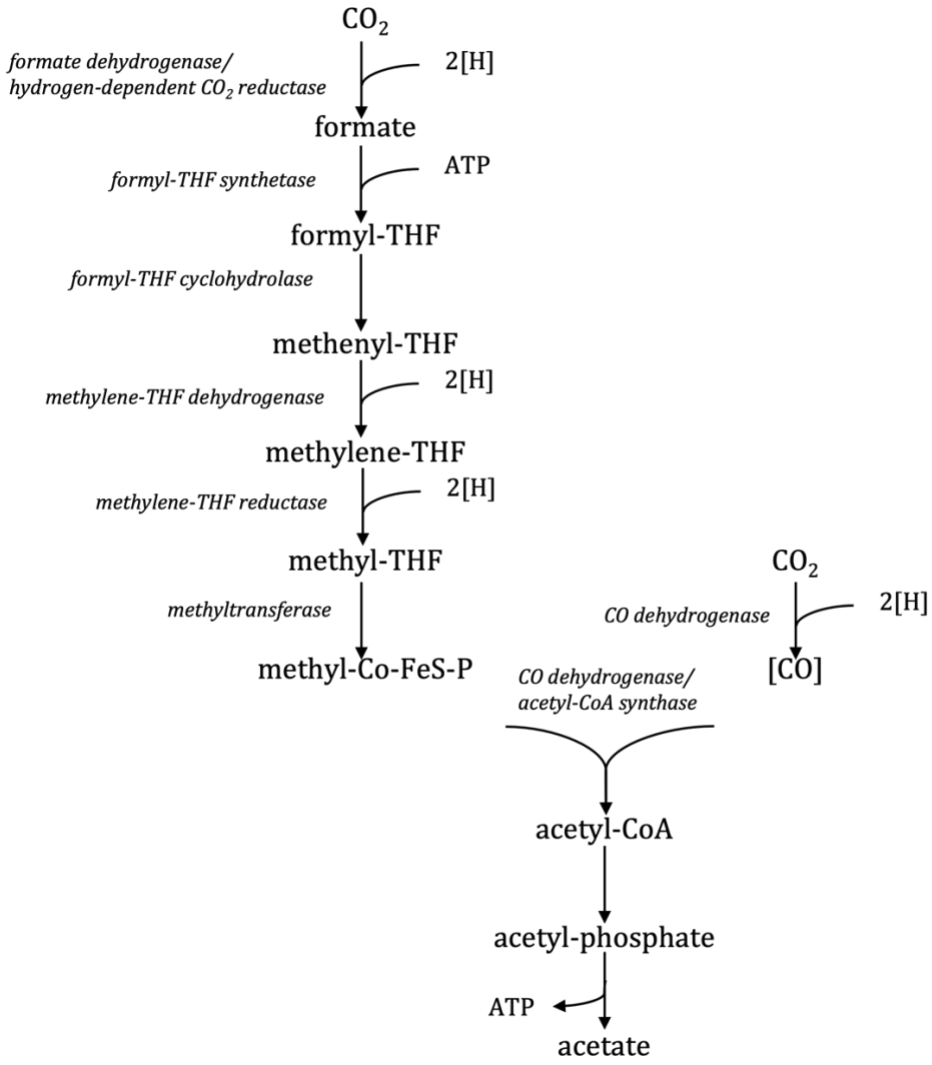

Figure 1.2**:** *The Wood-Ljungdahl-Pathway in acetogenic bacteria. CO_2 is converted through a series of steps into acetate and ATP. Adapted from (64)*

Compared to traditional thermochemical methods, biological H_2 production and CO_2 reduction have the great advantage of offering lower energy costs, greater carbon-neutrality and being based on renewable resources (65).

1.4 Biohybrid systems for the production of value-added chemicals from sunlight

1.4.1 The concept of a biohybrid system

Whilst biological light harvesting efficiency is often exceeded by solid state semiconductor light absorbers (66), the storage into chemical bonds of the photoexcited electrons and resulting energy remains a difficult task for abiotic catalysts, particularly in reference to the conversion of CO_2 into multicarbon compounds (67,68). The emerging field of "semi-artificial photosynthesis" thus seeks to fuse light harvesting particles with biocatalysts, either in the form of enzymes or microorganisms, for the production of fuels or chemicals (20). The earliest hybrid systems of materials and microorganisms included for example microbial fuel cells, in which electrogenic bacteria would be cultured on simple conductive electrodes for the generation of electricity (69).

Typically, an inorganic (photo-)electrode or photosensitiser produces a biologically available reducing equivalent as a result of the direct absorption of solar energy, for example in the form of an electrical current or a small-molecule mediator. This is then passed on to the biological aspect of the hybrid system, either the enzyme or microbe, where it is used to drive the catalysis of metabolic pathways such as for the reduction of CO_2 or H_2O into value-added products. These can vary from polymers, to organic acids all the way to fuels (70). For the successful production of solar fuels and efficient solar-to-chemical conversion, the biohybrid systems need to be highly efficient at capturing solar energy as well as providing low kinetic barriers to catalytic reactions with high selectivity (66).

1.4.2 Enzymatic biohybrid systems

In enzymatic biohybrid systems for light-driven biotransformations, there are normally two possible modes: a mediated mode between photocatalyst and enzyme, in which redox compounds transfer the reducing equivalents to the enzyme, or a direct contact mode, in which the enzyme and photocatalyst bind directly, enabling direct transfer of the photo-excited electrons (71).
For example, the light-driven reduction of N_2 into ammonia was successfully achieved by a biohybrid system of cadmium sulfide (CdS) nanorods with an iron-molybdenum [FeMo]-nitrogenase from nitrogen-fixing bacteria, leading to the production of the industrial fertiliser ammonia (NH_3) (72).

For the light-driven production of H_2, a variety of biohybrid systems using hydrogenases have been successfully applied. Hydrogenases are classified into three main groups, according to the transition metal ion composition at their active sites (44,73). The classifications are the following: the nickel-iron

([NiFe]), diiron ([FeFe]), and finally the monoiron, FeS-cluster-free iron [Fe]-hydrogenases. The most well-studied class of the three is the [NiFe]-hydrogenases, within which most enzymes tend to show a bias favouring H_2 oxidation(73). Many successful studies pairing hydrogenases with the semiconductor TiO_2 have been conducted for successful light-driven H_2 production (74–79).

Light-driven H_2 production was also achieved using carbon dots (CDs) with L-aspartic acid as a photosensitiser in a biohybrid system with the [FeFe]-hydrogenase isolated and artificially maturated from *Chlamydomonas reinhardtii* in the presence of the electron shuttle methyl viologen (MV) (80). A complex of purified [FeFe]-hydrogenase from *Clostridium acetobutylicum* with CdS nanorods showed promising results for photochemical H_2 production in a study by Brown et al. (81).

Other successful light-driven H_2 production assays using CDs were conducted by Hutton et al., simultaneously achieving biohybrid systems with a fumarate reductase for light-driven succinate production through the hydrogenation of fumarate (82). Using CdS nanorod biohybrid systems, capped with 3-mercaptopropionic acid and the [FeFe] hydrogenase 1 from *Clostridium acetobutylicum*, Brown et al. successfully achieved photocatalytic H_2 production (81).

Many applications for artificial photosynthetic CO_2 reduction have been achieved using biohybrid systems and the formate dehydrogenase enzyme (FDH), which catalyses the reduction of CO_2 into formate (83). Formate is a product with good stability formed in the reduction of CO_2, and is used in fuel cells, as a liquid energy carrier, a H_2 storage compound, as well as a feedstock for fine chemical synthesis (84).

For example, the immobilization of FDH-viologen, containing a long alkyl chain for the light-driven reduction of CO_2 to formic acid was achieved on an indium-tin oxide electrode by Amao & Shuto (85). FDH from *Desulfovibrio vulgaris* Hildenborough was also successfully coupled to metal oxides, namely porous indium-doped tin oxide as well as a TiO_2 electrode, leading to photocatalytic CO_2 reduction in the absence of an electron shuttle in a study conducted by Miller et al. (86)

Photoelectrochemical CO_2 reduction to formate using FDH in a hybrid system with a photocathode of CdS-modified copper indium sulfide ($CuInS_2$) and in the presence of MV was achieved by Toyodome et al. in 2021 (87). Further systems have been successful, such as systems coupling FDH to nanoporous carbon (88) or combining with water-soluble zinc porphyrin (89). Photocatalytic enzymatic hybrid systems have successfully been used for further assays in the reduction of CO_2, fixation of N_2, and for the synthesis of value-added chemicals (72,90,91).

Combining enzymes in photoelectrochemical setups in vitro however leads to issues with enzyme stability, as they are purified and expected to work outside of their natural uniquely protective environment and thus losing synergistic interaction with other proteins and organelles in their host cell (92). Furthermore, purification processes are energy demanding and cost intensive and the coupling of purified enzymes to photoelectrodes is often reliant on advanced technological procedures (93).

1.4.3 Whole-cell biohybrid systems

Microbial hybrid systems are attracting more and more interest, as the environments to allow stable growth of most of these organisms are easy enough to provide, enabling the enzymatic machinery necessary for the catalytic conversion to remain embedded in optimum conditions with high regeneration and repair potential. This increases the possibility for the synthesis of more complex target chemicals, higher stability and thus an increase in potential scalability. The downside, however, is that the process is subject to the organisms metabolic priorities, with survival ranking naturally higher than the selective production of any desired target chemicals (reviewed in (20)).

One of the early examples of successful microbial photoelectrosynthesis was achieved by Liu et al., in which solar-to-chemical conversion occurred through the creation of a *Sporomusa ovata* biohybrid system loaded into light-harvesting Si and TiO_2 nanowire photoelectrochemical cells, leading to CO_2 reduction to acetate and subsequent conversion of the acetate into fuels, pharmaceuticals and polymers by genetically altered *Escherichia coli* (94).

The successful photocatalytic H_2 production using a microbial biohybrid system was achieved by Honda et al. in 2016 (95). Using a recombinant *E. coli* strain expressing the [FeFe]-hydrogenase and relevant maturases from the acetogenic *Clostridium acetobutylicum* NBRC 13948, they were able to create a biohybrid system with TiO_2, and in the presence of the electron shuttle MV achieved successful photocatalytic H_2 production. The work was continued in 2017 (96) and represents some of the earliest successful examples of whole-cell reactions using recombinant *E. coli* for the photocatalytic production of H_2.

The light-driven production of H_2 and simultaneous reduction of fumarate, CO_2 and pyruvate using water-soluble photosensitisers in a biohybrid system was equally achieved by Rowe et al. using *Shewanella oneidensis* in the presence of MV (97).

1.5 Self-photosensitised biohybrid systems with self-generated semiconductors

1.5.1 The concept of self-photosensitisation

Whilst efforts have been made to genetically enhance naturally photosynthetic cyanobacteria for the production of biofuels (98), the metabolic pathways found in non-photosynthetic microorganisms are often energetically favourable for the process of fuel and chemical production, particularly the WLP for carbon fixation (99). The ability of microorganisms to precipitate toxic metal ions as a protective

response, leading to the creation of inorganic nanoparticles at their surface, is a well-known process (100).

CdS is an excellent and one of the most prominent semiconductors employed in photocatalytic biohybrid systems thanks to its broad absorption of the visible light spectrum (101). The enzyme cysteine desulfhydrase produces sulfide from cysteine and is found in a variety of microorganisms (102,103). The resulting sulfide then reacts and precipitates metal ions such as Cd^{2+}, leading to the production of homogenous CdS nanoparticles, which are predominantly anchored to the bacterial cell membrane (63).

Further to providing a sulfur source, cysteine also acts as a hole scavenger, replenishing the electron holes left behind by photoexcitation on the semiconductor. The oxidation of cysteine to cystine therefore contributes to the charge separation at the interface of the inorganic nanoparticle with the cell (63). Following biogenic nanoparticle creation, the self-photosensitised biohybrid systems are now able to catalyse the production of valuable products such as H_2 or other chemicals of interest (Fig. 1.3).

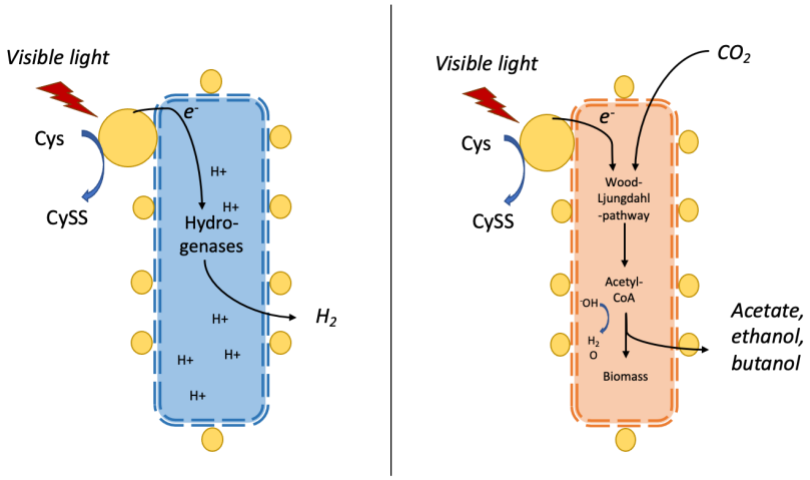

Figure 1.3: *Schematic representation of a self-photosensitised microbial biohybrid system, producing H_2 (left) or carbon products using the Wood-Ljungdahl-pathway for CO_2 fixation (right).*

1.5.2 Existing self-photosensitised microbial biohybrid systems

A highly significant break-through in the field came from a study by Sakimoto et al. (104), in which self-produced CdS-nanoparticles precipitated at the cell membrane were shown to successfully lead to the self-photosensitisation of the non-photosynthetic *Moorella thermoacetica* bacterium, with the hybrid system allowing for the successful and highly selective photocatalytic conversion of CO_2 into acetic acid (104). Equally, the light-driven reduction of CO_2 was achieved in the self-photosensitised *Methanosarcina barkeri*-CdS biohybrid, allowing for direct conversion of CO_2 into methane (CH_4), a promising energy carrier with an intrinsic calorific value of 890 kJ/mol (105).

Biohybrids developed using whole cells have further shown promising results for the production of H_2 under visible light, as exemplified in biohybrid systems of the facultative anaerobe *E. coli* following self-photosensitisation with self-precipitated CdS-nanoparticles (106), as well as in a hybrid system with the binary nanocomposite $AgInS_2/In_2S_3$, in which indium(III) sulfide (In_2S_3) nanoparticles were biosynthesised on the bacterial cell wall by the addition of In^{3+} and cysteine in the medium, and silver-indium-sulfide ($AgInS_2$) nanoparticles underwent *in situ* ion exchange on the surface of In_2S_3 nanoparticles (107).

Successful self-photosensitisation in *E. coli* through the precipitation of CdS nanoparticles led to H_2 production, which was further improved upon anaerobic induction of the indogenous [NiFe]-hydrogenase, and the system was equally able to generate a small amount of H_2 from waste water and natural sunlight (106). *In situ* biosynthesis of CdS nanoparticles further led to continuous H_2 production over 96 hours in a study by Wei et al. (108).

Due to the large part of biocatalytic activity occurring in the cytoplasm of microorganisms, the transport across the membrane of redox shuttle molecules is an additional energy consuming step with regards to extracellular semiconductors, leading to potential bottlenecks in transmembrane diffusion (109). In the search for different semiconducting materials, Zhang et al. (110) achieved the creation of a hybrid system using *M. thermoacetica* with cellularly uptaken gold nanoclusters (AuNCs). In comparison to CdS, these have the advantage of a higher cellular uptake, rather than being predominantly anchored to the membrane, and can easily permeate the *M. thermoacetica* cellular structures, therefore potentially facilitiang rapid mass transport and the electron transfer to the metabolic machinery. Zhang et al. found an improved cell viability, biocompatibility and quantum yield from the system using the AuNCs when compared to the *M. thermoacetica*-CdS biohybrid system. Biorecovery of gold has previsously equally been demonstrated in *E. coli* and *Desulfovibrio* spp. (111), suggesting the potential for AuNC based biohybrid systems in future assays as a semiconductor.

Shewanella loihica PV-4 has equally been shown to be capable of the synthesis of ultra-small nanoparticles from gold, and successful performance in the decomposition of dye (112). However, this system has not yet been studied for the light-driven production of H_2.

In a further successful assay of light-driven biohydrogen production, Luo et al. (2021) constructed a periplasmic photosensitised biohybrid system (PPBS), in which $CuInS_2$/ZnS quantum dots (QDs) were successfully taken up into the periplasmic space of the gram-negative bacterium *S. oneidensis* MR-1 for the production of H_2 (113).

1.5.3 Optimisation of existing biohybrid systems and novel value-added chemical production from photocatalysis

The area of semi-artificial photosynthetic solar-to-chemical conversion being relatively young, more work is needed to assess potential microorganism / semiconductor combinations in order to find the optimal systems for large scale applications. Recent work conducted in the BEM laboratory by Martins et al. investigated the self-photosensitisation of *Desulfovibrio desulfuricans, Shewanella oneidensis, E. coli* and *Citrobacter freundii* with CdS nanoparticles for light-driven H_2 production (114). Martins et al. found that the biohybrid system of *D. desulfuricans*-CdS was the most efficient at light-driven H_2 production compared to the other microorganisms and when compared to the model organism *E. coli*. Whilst all three novel biohybrid systems were able to produce H_2 using cysteine as a sacrifial electron donor, *D. desulfuricans*-CdS outperformed all other systems both in the presence as well as in the absence of an electron shuttle, continuously producing H_2 over the course of 10 days and achieving a high apparent quantum yield (AQY) of 23% in the presence of an electron mediator and 4% in its absence.

The work conducted in this thesis will therefore be based on this system and attempts to further optimise the biohybrid system for the light-driven production of H_2 as well as creating a new one for photoconversion of CO_2 into valuable compounds, namely the H_2 storage compound formate. This is to the best of my knowledge one of the first attempts at a microbial biohybrid system for the production of formate from CO_2.

2 Objective

The objective of this thesis is the creation of novel biohybrid systems displaying photocatalytic activity for the production of solar fuels, particularly the light-driven production of biohydrogen and the conversion of CO_2 into value-added compounds using two *Desulfovibrio spp*., namely *D. desulfuricans* and *D. vulgaris* Hildenborough.

Additionally, the role of specific enzymes, namely of the Hys [NiFeSe]- hydrogenase on the production of H_2, and of the FdhAB formate dehydrogenase in the reduction of CO_2 in *D. vulgaris* Hildenborough will be assessed.

3 Materials and Methods

3.1 Bacterial strains and growth conditions

3.1.1 Microorganisms

In this work, two strains of gram-negative sulfate-reducing bacteria were used; *Desulfovibrio vulgaris* Hildenborough (DSM 644) and *Desulfovibrio desulfuricans* ATCC 27774. Three different mutant strains of *D. vulgaris* Hildenborough were further used for the assessment of the role of hydrogenases and FDHs in H_2 production and CO_2 reduction respectively, namely a ΔfdhAB deletion mutant (115) , a ΔfdhAB+FdhAB^{rec} strain, created by assembly of the deletion mutant with a pRec-FdhAB-Strep complementation (83), as well as a Δhys100 strain(116).

3.1.2 Growth conditions

Desulfuvibrio spp. used in this thesis were grown anaerobically with N_2 gas headspace in 120 ml serum bottles containing a working volume of 50 ml of modified Postgate Medium C, containing (g L^{-1}); 4.5 sodium lactate, 2.5 Na_2SO_4, 1 NH_4Cl, 1 yeast extract, 0.5 KH_2PO_4, 0.3 sodium citrate tribasic dehydrate, 0.1 ascorbic acid, 0.1 sodium thioglycolate, 0.00016 resazurin, 0.06 $CaCl_2.2H_2O$, 0.06 $MgSO_4.7H_2O$, and 0.0071 $FeSO_4.7H_2O$.

Before inoculation, flasks were gassed with N_2 for 20 minutes to remove oxygen and create anaerobic conditions. The flasks were then sealed with butyl rubber stoppers and aluminium crimp seals and autoclaved, to sterilise the medium and remove any remaining oxygen. The anaerobic flasks were inoculated with 10% of the bacterial pre-inoculate and grown for 18 hours at 37°C in static conditions. Cell growth was determined through optical density at 600 nm (OD_{600}) on an Ultrospec 10 Cell Density Meter.

Mutant strains that required growth in the presence of an antibiotic were grown with 100 µg/ml of spectinomycin added to the growth media and grown for 24 hours (ΔfdhAB and Δhys100) and 48 hours (ΔfdhAB+FdhAB^{rec}).

3.2 Microbial-based biohybrid systems construction

3.2.1 Synthesis of monovalent *Desulfovibrio-CdS* and bivalent *Desulfovibrio-CdS-MoS_2* biohybrids

Cells of *Desulfovibrio spp.* were grown in 50 ml of sterile anaerobic Postgate medium C as described above but with the following modifications: without phosphate, and supplemented with 1 μM nickel chloride and 1 μM sodium selenite. For assays with mutant strains, the medium was further supplemented with 1 μM of tungsten. This medium will be denominated as BioCdS. The cells were incubated for 18 hours at 37°C in static conditions to obtain on OD_{600} of 0.7 for *Desulfovibrio desulfuricans* and 1.0 for *Desulfovibrio vulgaris* Hildenborough. Following growth, 3 mM of $CdCl_2$ was slowly added, whilst gently swirling the flasks to ensure even precipitation amongst the cells. The formation of CdS was observed by the formation of a yellow colour. The cells together with the metal were then incubated for a further 3 hours at 37°C to create the biohybrid.

For the synthesis of the *Desulfovibrio*-$CdSMoS_2$ biohybrid system, different amounts of molybdenum (as Na_2MoO_4) were added to evaluate the potential impact of Mo as a co-catalyst, with concentrations ranging from 0.003-0.5 mM. Synthesis was carried out following the same steps as for the singular biohybrid, with the addition of Mo immediately following the addition of $CdCl_2$ to the flask. In this case, the observed colour was slightly more orange than yellow.

3.2.2 Synthesis of the biohybrid system coupled to Pt and Pd biogenic nanoparticles

First the *Desulfovibrio*-CdS-biohybrid was synthesised according to the conditions laid out in 3.2.1. These biohybrids were collected and then coupled with BioPd or BioPt synthesised biologically as described in point 3.2.3. The BioPd and BioPt were centrifuged, recovered and concentrated in 100 μl and introduced into the photocatalytic flasks together with the *Desulfovibrio*-CdS-biohybrid.

3.2.3 Biological production of Pt^0 and Pd^0 nanoparticles

Pt^0 and Pd^0 nanoparticles were biologically produced using three different microorganisms, *Shewanella oneidensis*, *Desulfovibrio vulgaris* Hildenborough and *Desulfovibrio desulfuricans*.

The synthesis of BioPt and BioPd was performed using 50 ml of anaerobic metal solution (100 mg/L Pt or Pd at pH = 3). The cells were added to the solution in order to achieve a ratio of dry weight cells / metal of 3:1.

S. oneidensis cells were grown aerobically overnight in LB media and harvested by centrifugation for 10 minutes at 4000 rpm. Cells were then resuspended in 1 ml of sterile anaerobic 20 mM Tris-HCl buffer pH 7.6 and introduced into 50 ml anaerobic sealed flasks containing the metal solutions. In the case of *Desulfovibrio spp.* cells were grown anaerobically in the Postgate Medium C, collected at the end of log phase and harvested by centrifugation for 10 minutes at 4000 rpm. Following centrifugation, cells were washed twice with 10 ml of sterile anaerobic 20 mM Tris-HCl buffer pH 7.6 to remove any hydrogen sulfide (H_2S). After the final wash, the cells were resuspended in 1ml of sterile anaerobic 20 mM Tris-HCl buffer and transferred into a 50 ml anaerobic sealed flask containing the metal solutions. The flasks containing the cells and metal solution were then incubated for a further 20 minutes at 37°C (*Desulfovibrio spp.*) and 30°C (*Shewanella oneidensis*) and then gassed with H_2 for 5 minutes as the electron donor for the reduction of Pt^{4+} to Pt^0 and Pd^{2+} to Pd^0 respectively by the cells. Finally, cells were incubated at 37°C (*Desulfovibrio spp.*) and 30°C (*Shewanella oneidensis*) overnight in static conditions with an overpressure of 1 bar H2 (117).

3.3 Photocatalytic assays

3.3.1 Light-driven H_2 production

Assays for the light-driven production of H_2 were performed in photocatalytic glass flasks of 10 ml volume with a magnet inside. The flasks were initially sealed and purged for 10 minutes with N_2 to achieve anaerobic conditions. They were then filled with 5.5 ml of photocatalytic solution (pH= 2.3) containing anaerobic 20 mM Tris-HCl buffer (pH = 7.6), 0.8 µM resazurine and 2.85 mM cysteine. HCl-cysteine (0.5 ml) was also added to act as the sacrificial electron donor. Different cysteine concentrations were tested from 2.6 mM to 152 mM of cysteine.

Following the biohybrid synthesis, 22.5 ml of the *Desulfovibrio*-CdS- or *Desulfovibrio*-CdS-Mo-biohybrid were harvested by centrifugation at 4000 rpm for 10 minutes, resuspended in the photocatalytic solution and further washed by centrifugation at 5800 rpm for 8 minutes. Following this wash, the biohybrid was resuspended in 500 µl of photocatalytic solution and added into the photocatalytic flask.

For assays including BioPt/BioPd nanoparticles, the required amounts of the BioPt/BioPd nanoparticle solution were centrifuged for 10 minutes at 4000 rpm, resuspended in 100 µl of photocatalytic solution and added to the photocatalytic flask.

The flasks were incubated on a magnetic stirrer plate under violet LED lighting.

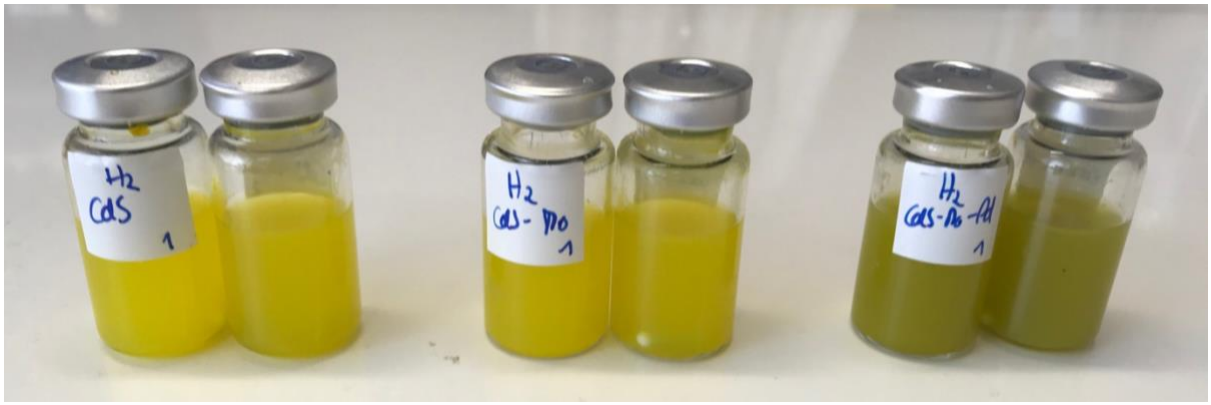

***Figure 3.1**: Example of photocatalytic flasks containing duplicates of different Desulfovibrio-biohybrid systems for light-driven H_2 production assays*

3.3.2 Light-driven CO_2 reduction

Assays for the light-driven reduction of CO_2 were performed in photocatalytic glass flasks of 10 ml volume with a magnet inside. The flasks were initially sealed and gassed for 10 minutes with N_2 to achieve anaerobic conditions. Due to the novelty of the experiment and the absence of previous data, experiments were carried out both in the presence and absence of an electron shuttle MV. The photocatalytic flasks for assays in the presence of the electron shuttle were filled with 4 ml of photocatalytic solution and 4.5 ml for assays in the absence of the electron shuttle. The photocatalytic solution was prepared as for assays of H_2 production (see 3.3.1). HCl-Cysteine (81 mM) was added in assays for CO_2 reduction as a sacrificial electron donor. In corresponding assays, 500 µl of MV were added. Furthermore, 100 mM of sodium hydrogen carbonate was added as a CO_2 source. Depending on the assay, BioPt / BioPd nanoparticle solution were added.
The flasks were incubated on a magnetic stirrer plate under violet LED lighting.

3.3.3 Photoreactor setup for light-driven H_2 production and CO_2 reduction

A bench-scale photoreactor was set up for assays on the scalability of the previously identified optimised biohybrid systems for both the light-driven production of H_2 as well as the reduction of CO_2 (Fig. 3.2). The reactor was conducted in batch mode in a long 750ml glass flask with gas / liquid outlets with a magnet inside, and placed at 4°C on a stirrer plate to keep the internal temperature at 40°C. Conditions in the reactor were an exact scale up from the 10 ml photocatalytic flasks to a working

volume of 400 ml. It was initially filled with the photocatalytic buffer and then gassed with N_2 for 1 hour to achieve anaerobic conditions. After sealing the SED and, in the case of CO_2 reduction assays MV and the sodium hydrogen carbonate solution were added.

***Figure 3.2**: Bench-scale reactors for the light-driven production of H_2 (left) and the light-driven reduction of CO_2 (right)*

3.4 Light source characterisation

The assays were carried out with the photocatalytic flasks attached to the bottom of a 5 L glass beaker, lined with light emitting diode (LED) chains and covered from the outside with aluminium foil. The beaker was placed at 4°C on top of a magnetic stirrer plate, with an internal temperature of 37°C (Fig. 3.3).

Assays of H_2 production were conducted with violet LEDs emitting a wavelength of λ= 445 nm (visible spectrum) with an intensity of 0.42 Wm^{-2}. Assays of CO_2 reduction were carried out in the same setup, but with LEDS emitting a wavelength of 445 nm with an intensity of 3.8 Wm^{-2}. The bioreactor was wrapped with circular LED light chains with a light intensity of 2.1 Wm^{-2} and a wavelength of 445 nm.

In order to allow for the conduction of electrons, the supplied energy by the light source needs to be superior to the band gap of the semiconductor CdS (E_g = 2.38 eV)(118). At a wavelength of 445 nm, the energy emitted by the violet LEDs corresponds to an energy value of 2.52 – 2.84 eV (119).

***Figure 3.3**: Photocatalytic flasks in experimental setup arranged within 5 L glass beaker (right) under violet LED irradiation (left)*

3.5 Analytical methods

3.5.1 H_2 quantification by gas chromatography

The concentration of photocatalytically produced H_2 was determined using gas chromatography (GC), by analysing an injected volume of 30 µl of headspace gas into a TRACE GC Ultra (Thermo) with a MolSieve 5A 80/100 column (Althech) and a thermal conductivity detector (TCD), at 130°C for 3-minute cycles and N_2 as the carrier gas with a flow rate of 10 ml / min. The calibration curve to convert the resulting areas into µmol of molecular hydrogen was done by injecting 30 µl of headspace gas from a 10 ml flask containing a working volume of 6.5 ml photocatalytic buffer and known amounts of H_2, starting at 0 µl and gradually increasing to 2000 µl. The resulting area was measured at the peak (Tr = 1.13min) after each injection. The volume injected was converted into moles of hydrogen using the equation for perfect gases:

$$P \times V = n \times R \times T \qquad \text{(Equation 1)}$$

Where P=1 atm, V = injected H_2 volume, R=0.082057 atm*L/mol*k, T= 298K .

The resulting calibration curve (Fig. 3.4) led to the following equation for the conversion of obtained area into moles of H_2:

4×10^{-6} x measured area = µmol H_2 (Equation 2)

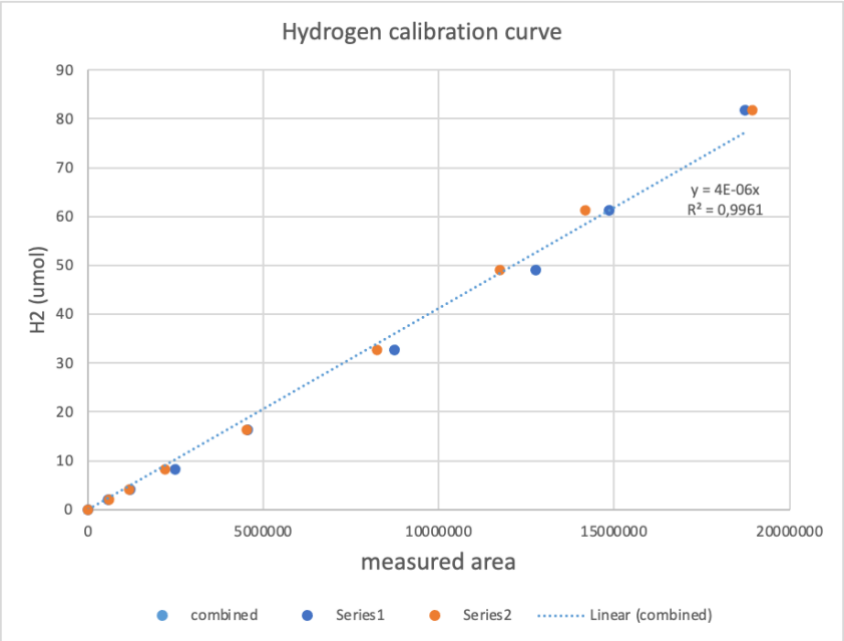

Figure 3.4**:** *H_2 calibration curve used to determine the amount of H_2 produced in light-driven assays. Series 1 and 2 represent two independent experiments.*

The H_2 production of the biohybrid systems was determined by periodic sampling for up to 6 consecutive days and conversion of the resulting area into moles of H_2 according to the calibration curve. The H_2 production rate (µmol h^{-1}) was determined by dividing the produced concentration by the irradiation time (h). H_2 production specific rate (µmol g_{dcw}^{-1} h^{-1}) was determined by correlating produced concentration (µmol) with g_{dcw} (determined by OD_{600}) and dividing by the irradiation time.

3.5.2 Quantification of organic compounds by high performance liquid chromatography

Analysis of organic compounds was carried out by high performance liquid chromatography (HPLC), with an Alliance 2695 Waters chromatographer, which was connected to a Waters Absorbance Detector (both Waters Chromatography, Milford, MA) set at 195 nm. Data acquisition was carried out using the Empower 2 software (Waters Chromatography, Milford, MA), and chromatographic separation

accomplished using an Aminex HPX-87H column (300 x 7,8 mm), with a particle size of 9 µm (Bio-Rad, Hercules, California), set at 45°C. Compound elution was done isocratically with a flow rate of 0.6 $mL \cdot min^{-1}$, with 0.005 N of H_2SO_4 and an injected sample volume of 100 µl. The retention times for the three analysed components lactate, formate and acetate were 12.8 minutes; 13.9 minutes and 15 minutes respectively.

3.5.3 Determination of cell weight

Dry cell weight (g_{dcw}) was determined through the measurement of the optical density at 600 nm (OD_{600}) using a Shimadzu UV/Vis spectrophotometer and the correlation between optical density and dry cell weight that was already determined in previous work. For *Desulfovibrio spp.*, a value of OD_{600} = 1 corresponded with 0.31 $g_{dcw}L^{-1}$ (120).

3.6 Biohybrid characterisation

To characterise the *Desulfovibrio*-CdS-MoS_2 and *Desulfovibrio*-CdS-MoS_2 + BioPd biohybrid systems and gain insights into the distribution and relationship between the semiconductor particles and the cells, scanning electron microscopy (SEM), transmission electron microscopy (TEM), and SEM and TEM coupled to energy dispersive spectroscopy (SEM-EDS and TEM-EDS) were carried out.

3.6.1 SEM and TEM characterisation of biohybrids

The *Desulfovibrio*-biohybrid was collected and centrifuged for 10 minutes at 4400 rpm. The pellet was then washed in 1 ml of 20 mM Tris-HCl buffer. Following centrifugation, the biohybrid was fixed in 1 ml fixation solution (2.5% glutaraldehyde, 2% formaldehyde in 20mM Tris-HCL buffer) overnight at 4°C. The following day, cells were washed 3 times in 1 ml of 20 mM Tris-HCl buffer by centrifugation at 4400 rpm for 3 minutes after a 7 minute incubation period at room temperature. After the third wash, cells were fixated in 500 µl of 1% osmium in 20 mM Tris-HCL Buffer and left on ice for 1 hour. Cells were washed a further 3 times in 1 ml of 20 mM Tris-HCl buffer and centrifuged at 4400 rpm for 3 minutes after a 7 minute incubation at room temperature. Following this wash, progressive dehydration steps were carried out with 1 ml of ethanol, being incubated for 7 minutes at room temperature and then centrifuged for 3 minutes at 4400 rpm, using the following concentrations in ascending order: 30%,

50%, 75%, 90% and finally three cycles of dehydration with 100% ethanol. The Eppendorf tubes containing the dry biohybrid were then placed in liquid nitrogen followed by overnight lyophilization. Collected samples were sent to be analysed and were attached onto an A1 stub with double-sided carbon tape. A thin film consisting of Au / Pd was then applied to the surface with a Quorum Technologies model Q150T ES. Visualization of the samples was done with a FEG-SEM JEOL JSM7001F and a Hitachi H8100 TEM. For SEM-EDS, a light elements Si (Li) detector (Oxford, model INCA250) was used.

3.6.2 X-ray diffraction and transmission electron microscopy characterisation of the dried biohybrid systems

To determine the crystalline structure and the size and morphology of the biogenic semiconductor nanoparticles, the *Desulfovibrio*-CdS- and *Desulfovibrio*-CdSMoS_2-biohybrids as well as *Desulfovibrio*-BioPd nanoparticles were prepared for analysis by X-ray diffraction (XRD) and TEM-EDS. The biohybrids and nanoparticles were collected and centrifuged for 10 minutes at 4400 rpm. The pellets were then resuspended in 1 ml of 20 mM Tris-HCl and centrifuged for a further 5 minutes at 13000 rpm. Pellets were left to dry out overnight in the 65°C incubator. The following day, the pellets were pulverised using a pestle and mortar and stored in Eppendorf tubes to be analysed by XRD and TEM-EDS.
Unfortunately, due to constraints on the availability that were outside of our control, it was not possible to obtain results from XRD.

3.6.3 Apparent quantum yield

To determine the apparent quantum yield (AQY), the following equation was used:

$$\text{AQY (\%)} = \frac{number\ of\ electrons\ used\ to\ produce\ H_2}{number\ of\ incident\ photons} \text{ x } 100$$

$$\text{AQY (\%)} = \frac{\frac{2 \text{ x } C_{H2} \text{ x } N_A}{P \text{ x } A \text{ x } t \text{ x } \lambda}}{h \text{ x } c} \text{ x } 100 \qquad \text{(Equation 3)}$$

In the equation, C_{H2} (moles) corresponds to the amount of H_2 produced over the irradiation period (t, seconds). Avogrado's number (6.022 x 10^{23}) is denoted as N_A, the power density of the energy source as P (in Wcm^{-2}), the irradiation area (in cm^2) as A, the wavelength of light (in m) as λ, Planck's constant (6.63 x 10^{-34} J s) as h and the speed of light (3 x 10^8 m s^{-1}) as c. Although irradiation scattering and loss of reflection occurred due to the curved shape of the photocatalytic flasks, A was assumed to be equivalent to the surface of the entire flask (16.6 cm^2).

3.6.4 Equations used to determine molar balances of the processes

H_2 production:

$$2\ H^+ \xrightarrow{2e-} H_2$$

$$2\ Cys + 2\ H^+ \xrightarrow{2\ e-} H_2 + 1\ Cyss \qquad \text{(Equation 4)}$$

Formate production:

$$CO_2 + 2\ H^+ \xrightarrow{2e-} HCOOH$$

$$2\ Cys + CO_2 + 2\ H^+ \xrightarrow{2\ e-} HCOOH + Cyss \qquad \text{(Equation 5)}$$

Acetate production:

$$2\ CO_2 + 8\ H^+ \xrightarrow{8e-} CH_3OOH + 2\ H_2O$$

$$8\ Cys + 2\ CO_2 + 8\ H^+ \xrightarrow{8\ e-} CH_3COOH + 4\ Cyss + 2\ H_2O \qquad \text{(Equation 6)}$$

4 Results and Discussion

Providing an alternative to environmentally unfriendly energy as well as cost-prohibitive processes for the production of semiconductors, the nanoparticles in this thesis were biosynthesised by the organisms themselves. This occurs through precipitation of cadmium reacting with H_2S, which is produced by *Desulfovibrio spp*. through dissimilatory pathways (118,121). Biogenic nanoparticles such as the CdS attached to the cell surface form the *Desulfovibrio*-biohybrid systems used in this work, which have the advantage of a unique and very close interaction between the light-harvesting semiconductor and the microorganism, allowing for direct electron transfer from the excited semiconductor into the biological system (114) and successful self-photosensitisation.

4.1 Assays for the light-driven production of H_2

Assays for the light-driven production of H_2 follow up on experiments conducted with the *D. desulfuricans*-CdS biohybrid system, previously carried out in the BEM laboratory at ITQB and already published (114). The use of co-catalysts in photocatalytic water splitting has been shown to improve the quantum efficiencies of semiconductors through the trapping of photogenerated charges and the promotion of the charge separation, leading to an improvement of the photostability. Furthermore, one of the most important roles of the co-catalyst is in the lowering of the activation energy of the catalytic reaction (122).

4.1.1 Effect of BioPd and BioPt on light-driven H_2 production by the *D. desulfuricans*-CdS biohybrid system

Noble metals have traditionally been used as co-catalysts in the photocatalytic H_2 evolution in order to provide effective proton reduction sites as well as serving as electron sinks. For chemically synthesised semiconductors, previous work has shown an enhancement of performance when the semi-conductors were doped with metals from the platinum group acting as co-catalysts (123).
Previous work by the BEM laboratory showed the ability of *D. vulgaris* to reduce platinum (Pt) as well as palladium (Pd) and therefore create biogenic Pt- and Pd-nanoparticles (117). The resulting nanoparticles are denominated as BioPt and BioPd respectively. In order to explore their potential as co-catalysts and effect on light-driven biological H_2 production, assays were carried out combining BioPt and BioPd in various concentrations with the *Desulfovibrio*-CdS biohybrid systems.

Initial assays for examining optimum concentrations of BioPt and BioPd were also carried out with nanoparticles produced by *Shewanella oneidensis*.

Assays were conducted by adding 2 ml, 5 ml, 9 ml, 13 ml and 17 ml of the *S. oneidensis*-produced BioPt and BioPd nanoparticles concentrated to 0.1 ml of photocatalytic solution to the *D. desulfuricans*-CdS biohybrid (Fig. 4.4). After 46 hours, the *D. desulfuricans*-CdS biohybrid produced 12 ± 3 µmol of H_2. The *D. desulfuricans*-CdS biohybrid systems doped with BioPt and BioPd nanoparticles showed at least a 2.7-fold increase, reaching 32 ± 1 µmol with as little as 2 ml of the nanoparticle suspension. However, the improvement in H_2 production was not proportionate to the amount of nanoparticles used, with increases in nanoparticles only slightly improving H_2 yields in the case of BioPt (Figure 4.1A), and production yields slightly decreasing on average in the assays using BioPd (Figure 4.1B). This could be due to the electron transfer kinetics having already reached their maximum and therefore not being accelerated at higher concentrations of the BioPt and BioPd nanoparticles.

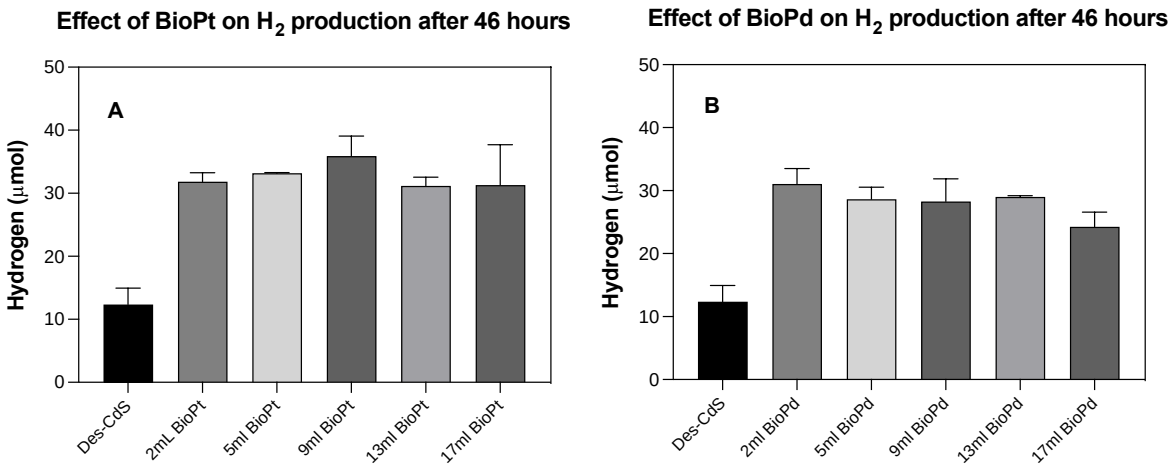

Figure 4.1: *Effect of different amounts of S. oneidensis BioPt (A) and BioPd (B) nanoparticle suspension on the light-driven H_2 production by the D. desulfuricans-CdS biohybrid system after 46 hours. Experiments carried out in duplicate; data shown as mean ± standard deviation.*

As metals of the platinum group are expensive, the amount used for sustainable H_2 production assays is an important factor. When assessing the efficiency of the production per ml, the use of 2 ml BioPt or BioPd was vastly more efficient when compared to higher concentrations. For the sustainability of long-time biological H_2 production, the cost associated with the experimental setup is an important factor to consider. Although palladium is rarer than platinum (124), at the time of the experiment, (January 2021), the platinum price was above the price for palladium. At the chosen volume of 2 ml BioPt / BioPd, H_2 production efficiency was effectively the same, hence it was decided to continue the assays with BioPd nanoparticles on the basis of a lower cost burden.

Desulfovibrio spp. produce H_2S, which inactivates platinum metal group nanoparticles (125). Although slightly more laborious, it is possible to carefully wash the cells to remove H_2S, and thus create *Desulfovibrio spp*. specific BioPt and BioPd instead of the previously used nanoparticles produced by *S. oneidensis*. To test the impact of heterologous vs homologous nanoparticle composition, the efficiency of light-driven H_2 production of the *D. desulfuricans*-CdS biohybrid with 2 ml of BioPd produced by *D. desulfuricans*, *D. vulgaris* Hildenborough and *S. oneidensis* respectively was compared. After 46 hours of light irradiation, the homologous *D. desulfuricans*-CdS + BioPd biohybrid produced 37 ± 2 µmol, the system with *D. vulgaris* BioPd nanoparticles produced 40 ± 4 µmol and the system with BioPd produced by *S. oneidensis* 33 ± 1 µmol of H_2 (Fig. 4.2). The H_2 production yield was within the same order of magnitude between the different types of BioPd, therefore, going forward, nanoparticles synthesised by the respective organisms to be used for the construction of the biohybrid would be used.

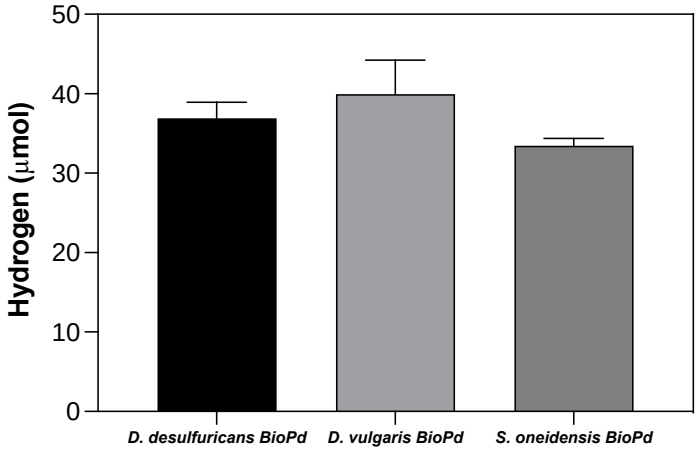

Figure 4.2: *Effect of 2ml of BioPd nanoparticles produced by three different microorganisms on the light-driven H_2 production of the D. desulfuricans-CdS biohybrid system after 46 hours. Experiments carried out in duplicate; data shown as mean ± standard deviation.*

Historically, Pt has been considered the best co-catalyst for H_2 evolution as it shows the lowest activation energy (122). The use of Pd in electrocatalysis has received less attention due to its comparatively lower stability and activity to Pt, however the cost of a co-catalyst is an important factor to consider and Pt has historically been more expensive than Pd (126). As observed in the experiments here, there was no disadvantage in using Pd over Pt, henceforth assays will be conducted with Pd.

4.1.2 Effect of cysteine concentration on light-driven H_2 production by the *D. desulfuricans*-CdS biohybrid system

One of the potential limiting factors in the production of light-driven H_2 is the concentration of the sacrificial electron donor (SED). The SED is paramount to quench the electron *holes* left behind on the semi-conductor following photo-excitation and electron transfer to the cell. For optimal turnover, the concentration of the SED present needs to be sufficient to allow for swift electron replenishment and therefore high H_2 production rate but may not be so high as to inactivate the cells. Therefore, the H_2 production under different concentrations of cysteine were assessed, ranging from 3 – 152 mM (Fig. 4.6).

As the concentration of cysteine increases, the rate of H_2 production increases, supporting the fact that at lower concentrations the SED is an important limiting factor in the production of H_2. While a higher concentration of cysteine does improve the performance of the photocatalytic system, it is however not the sole limiting factor. If this were the case, we would see a linear increase in production with higher concentrations of cysteine. However, what was observed is that the H_2 production and production rate improve initially and then begin to slowly plateau. It is therefore possible that the electron transfer within the cell and the kinetics of the hydrogenase enzymes might be important limiting factors. We determined the ideal cysteine concentration to be 81 mM, as it showed a strong H_2 production rate of 0.5 µmol/h and there was only a very minor improvement of both H_2 yield and production rate at higher cysteine concentrations (Fig. 4.3).

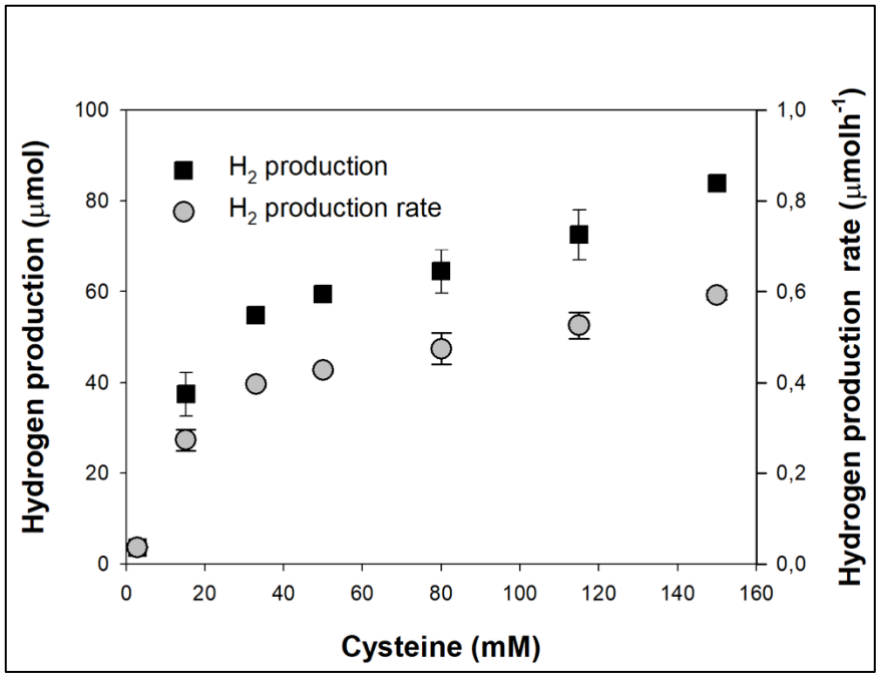

Figure 4.3: *Effect of the concentration of cysteine (the SED) on the yield of H_2 and the H_2 production rate of the D. desulfuricans-CdS biohybrid system. Experiments carried out in duplicate; data shown as mean ± standard deviation.*

The effect of the concentration of the SED on the performance of biohybrid systems has further been assessed in other studies. An improvement in the light-driven conversion by a *Methanosarcina barkeri*-CdS biohybrid of CO_2 to CH_4 at increasing cysteine concentrations was equally observed by Ye et al. (105). Zhang et al. tested the impact of the cysteine concentration in their 2018 study on the production of acetic acid in the *M. thermoacetica*-CdS and *M. thermoacetica*-AuNCs biohybrid systems. increasing the concentration from 17 mM to 25 mM did not improve the acetic acid production of the *M. thermoacetia*-CdS biohybrid, however an improvement was observed in the system photosensitised by the AuNCs (110). Which means that effect of Cysteine depends on the biohybrid systems.

4.1.3 Effect of molybdenum as a co-catalyst on the light-driven H_2 production by the *D. desulfuricans*-CdS biohybrid system

As mentioned, an important aspect in the construction of efficient photocatalytic systems based on CdS semiconductors is the use of co-catalysts, which can reduce the recombination of the photo-induced charges on the semiconductor as well as stimulate the charge transfer (127). Whilst these are often based on noble metals such as Pt, Pd, Au or Rh, in order to create cost-efficient and therefore sustainable systems, the search for efficient co-catalysts based on earth abundant non-noble metals is

important. The use of nickel-based materials such as Ni, NiO or NiS, or transition metals such as Cu and Fe have shown an enhancement of photocatalytic H_2 production (128). Recently, research into the use of MoS_2 as a co-catalyst has shown to have a positive impact on the H_2 production performance of CdS semiconductors, demonstrating excellent co-catalytic abilities (129).
Following on from previous work conducted in the BEM laboratory, the use of MoS_2 as a co-catalyst in the *D. desulfuricans*-CdS biohybrid system will be investigated here. To identify the optimal Mo concentration, assays were carried out using the *D. desulfuricans*-CdS biohybrid with the addition of different concentrations of Mo ranging from 0.003 mM to 0.5 mM during initial CdS formation. The successful precipitation of $CdSMoS_2$ was observed by a slightly more orange colour, darkening with increasing concentrations of Mo.

Whilst the H_2 yield was improved at all Mo concentrations, the biggest increase in H_2 production efficiency was observed with a 0.1 mM concentration of Mo in the *D. desulfuricans*-$CdSMoS_2$ biohybrid system. H_2 production after 45 hours increased from 12 ± 4 µmol in the biohybrid system lacking molybdenum to more than two-fold at a concentration of 0.1 mM Mo, producing 25 ± 4 µmol in the same amount of time (Fig. 4.4).

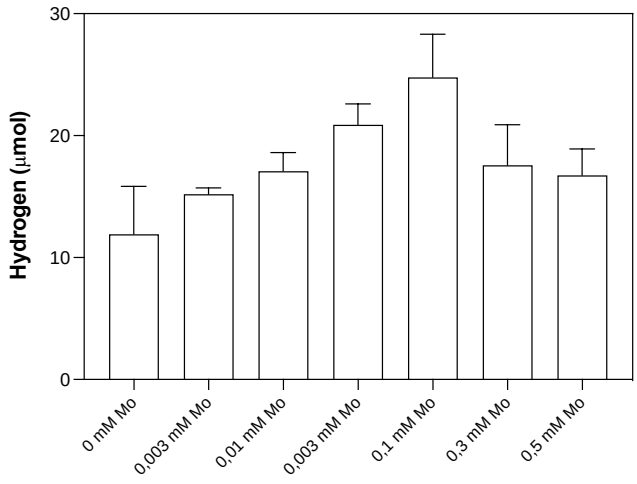

***Figure 4.4**: Effect of the Mo co-catalyst on the light-driven H_2 production by the D. desulfuricans-CdS biohybrid system after 45 hours. Experiments were carried out in duplicate; data shown as mean ± standard deviation.*

MoS_2 does not act as a semiconductor as it does not have photocatalytic abilities itself, but acts as co-catalyst (129). The better performance of the *D. desulfuricans*-$CdSMoS_2$ biohybrid system suggests an improvement in the electron transfer from CdS into the cell. At all given concentrations of Mo the performance of the biohybrid system improved, however, concentrations above 0.1 mM of Mo show a downward trend, suggesting toxicity of concentrations above 0.1 mM to the microorganisms.

The charge-transfer process between semiconductor, co-catalyst and biological catalyst is highly influenced by the geometry and strength of the molecular assembly behind the interfacial interactions, and the energetics, efficiencies and kinetics of the process can be optimised by exploring this field further (130).

In their assays with MoS_2, Zong et al. it was hypothesised the enhancement of the photocatalytic performance to be due to the intrinsic characteristics of the formed junctions between CdS and MoS_2, with their $CdSMoS_2$ semiconductor and co-catalyst even outperforming biohybrid systems of CdS based on other noble metals (129).

The use of co-catalysts equally increased the performance of other biohybrid systems. Doping CdS with Ni equally led to an improvement of the photocatalytic conversion of CO_2 to CH_4, with an approximately 250% higher yield in the *M. barkeri*-$Ni_{(0.75\%)}$:CdS biohybrid than in the singular *M. barkeri*-CdS biohybrid system, however these semiconductors were not biogenically produced (131). Coupling biogenic In_2S_3 nanoparticles to $AgInS_2$ nanoparticles equally led to an improvement in electrical conduction enhancing the performance of the AgInS2/ In2S3*@E.coli* biohybrid system when compared to In_2S_3 alone. This was thought to be through the improved utilisation of the photo-generated electrons and subsequent suppression of the recombination of the photogenerated charges (107). In chemical photocatalytic H_2 production, the performance of CdS had also been shown to be enhanced up to 7x through the presence of FeSe nanorods as co-catalysts (132).

In order to maximise potential H_2 production, a biohybrid system combining both co-catalysts and at the optimum cysteine concentration was created. BioPd works as a secondary cocatalyst which increases H_2 production by lowering the activation energy for H_2 production. It can also contribute by capturing the photogenerated electrons which contributes to suppress electron-hole recombination (122). The *D. desulfuricans*-$CdSMoS_2$+BioPd biohybrid system using 81 mM cysteine was able to produce 149 ± 8 µmol of H_2 after 141 hours. In comparison, the *D. desulfuricans*-CdS biohybrid only produced 64 ± 2 µmol and the *D. desulfuricans*-$CdSMoS_2$ biohybrid 105 ± 10 µmol of H_2, which is less than half. We therefore determined the optimum biohybrid system in the absence of an electron shuttle to be a *D. desulfuricans*-$CdSMoS_2$+BioPd biohybrid with 3 mm Cd, 0.1 mM Mo and 2ml of BioPd nanoparticles at a cysteine concentration of 81 mM.

The use of *Desulfovibrio spp.* for the photocatalytic production of H_2 in biohybrid systems is new, and to the best of my knowledge has up until now only been studied in the work by Martins et al. (114). In their work, the *D. desulfuricans*-CdS biohybrid system outperformed other self-photosensitised biohybrid systems constructed with *Citrobacter freundii*, *S. oneidensis* and *E. coli* in the photocatalytic H_2 production. In the presence of MV, the *D. desulfuricans*-CdS biohybrid system by Martins et al. achieved an AQY of 23% after 120 hours, which was higher than that reached in the majority of published biohybrid systems based on self-produced semiconductors (104–107,110). In the absence of

MV, the D. desulfuricans-CdS biohybrid system by Martins et al. only reached an AQY of 4% (114). The optimised *Desulfovibrio*-$CdSMoS_2$ biohybrid system at 81 mM in this work was however equally able to reach an AQY of 23% , after 141 hours of light irradiation in the complete absence of an electron shuttle, therefore greatly outperforming the previously reported *D. desulfuricans*-CdS system and proving very successful.

Of the other self-photosensitised biohybrids system used in the light-driven production of H_2, the system using *E.coli*-CdS only achieved an increase in the production of H_2 of approximately 30% when compared to the cells alone, corresponding to apparent quantum efficiencies (QE) of 7.93% and 9.59% at 470 and 620 nm of irradiation respectively. Furthermore, this was at a much higher intensity of visible light irradiation of 2000 Wm^{-2} (106). The biohybrid system based on the $AgInS_2/In_2S_3$*@E.coli* showed an even smaller QE of 3.3% at 720 nm (107). Additionally, both of these systems required the presence of glucose and other organic ingredients. In addition to outperforming the previously established self-photosensitised systems for the light-driven production of H_2, the *Desulfovibrio*-$CdSMoS_2$ + BioPd achieved a much higher AQY as systems reported for the light-driven reduction of CO_2 (104,105,110).

4.1.4 Comparison of light-driven H_2 production by the *D. desulfuricans*-$CdSMoS_2$ + BioPd and *D. vulgaris* Hildenborough-$CdSMoS_2$+BioPd biohybrid systems

The light-driven production of H_2 was compared between biohybrids constructed by the two *Desulfovibrio* spp, *D. desulfuricans* and *D. vulgaris* Hildenborough.

The simple *D. desulfuricans*-CdS biohybrid system outperformed the *D. vulgaris*-CdS biohybrid, with a H_2 production of 64 ± 2 µmol after 142 hours of light irradiation, compared with 14 ± 4 µmol after 142 hours for the latter. In the presence of the co-catalyst MoS_2, the *D. desulfuricans*-$CdSMoS_2$ biohybrid produced 105 ± 10 µmol, which is within the same order of magnitude to that obtained by the *D. vulgaris*-$CdSMoS_2$ biohybrid, which produced 93 ± 2 µmol of H_2. These results demonstrate that MoS_2 helps the transfer of electrons from the semiconductor to the cells. In the simple system, the electron transfer from the semi-conductor to the hydrogenases of *D. vulgaris* appears not to run as efficiently as it does in *D. desulfuricans*. However, in the optimal biohybrid systems of *Desulfovibrio*-$CdSMoS_2$+BioPd, there was no longer a difference between the effectiveness of the biohybrid systems, with *D. desulfuricans*-$CdSMoS_2$+BioPd producing 149 ± 8 µmol and *D. vulgaris*- $CdSMoS_2$+BioPd 148 ± 24 µmol (Fig. 4.5), both reaching an AQY of 23% (Eq. 3) after 141 hours and 142 hours respectively. As the electron transfer from the semiconductor into the cells metabolic enzyme machinery in the absence of an electron shuttle will be dependent on the organisms ability to transfer charges into the cell, it appears that the charge transfer process in *D. desulfuricans* is more efficient

than in *D. vulgaris*. However, this difference is circumvented by the presence of the co-catalysts, suggesting that their presence greatly facilitates the electron transfer from the light-absorbing semiconductor to the hydrogenases.

To test the reliance of the biohybrid system on the biological catalysis of active*Desulfovibrio* cells, assays were carried out with inactivated biohybrids as a control. To create the inactivated biohybrid system, the flasks containing the *Desulfovibrio*-biohybrid systems were autoclaved prior to the beginning of the irradiation experiments.
After 142 hours, the active biohybrid systems of *D. desulfuricans*-CdS, *D. desulfuricans*-CdSMoS_2 and *D. desulfuricans*-CdSMoS_2 + BioPd produced 64 ± 2 µmol; 105 ± 10 µmol and 148 ± 8 µmol of H_2 respectively. In contrast, the corresponding inactivated biohybrid systems only produced 2 ± 0 µmol, 11 ± 0 µmol and 14 ± 2 µmol of H_2 respectively (Fig. 4.5B). The inactivated *D. vulgaris*-CdS, *D. vulgaris*-CdSMoS_2 and *D. vulgaris*-CdSMoS_2 + BioPd biohybrid systems produced 1 ± 0 µmol, 14 ± 1 µmol and 18 ± 3 µmol respectively (Fig. 4.5D). This suggests that the CdS semiconductor has a low intrinsic ability of independent catalysis for H_2 production, with slightly improved performance in the presence of co-catalysts, but on a level that is much lower than in the presence of living *Desulfovibrio spp.* cells, which are the main catalyst.

Two further control experiments were carried out to better characterise the system and evaluate the role of the co-catalysts. Assays of *Desulfovibrio*-MoS_2 biohybrid systems, constructed in the absence of CdS but with 0.1 mM of Mo did not produce any H_2, confirming the action of Mo as a co-catalyst improving H_2 production, but its inability to act as a fully sufficient semi-conductor on its own. Equally, the simple suspension of *Desulfovibrio* cells without the CdS semi-conductor but in the presence of BioPd nanoparticles did not produce any H_2 (Fig. 4.5B & D). These results confirm that it is the *Desulfovibrio* cells that are the main catalyst responsible for the light-driven production of H_2.

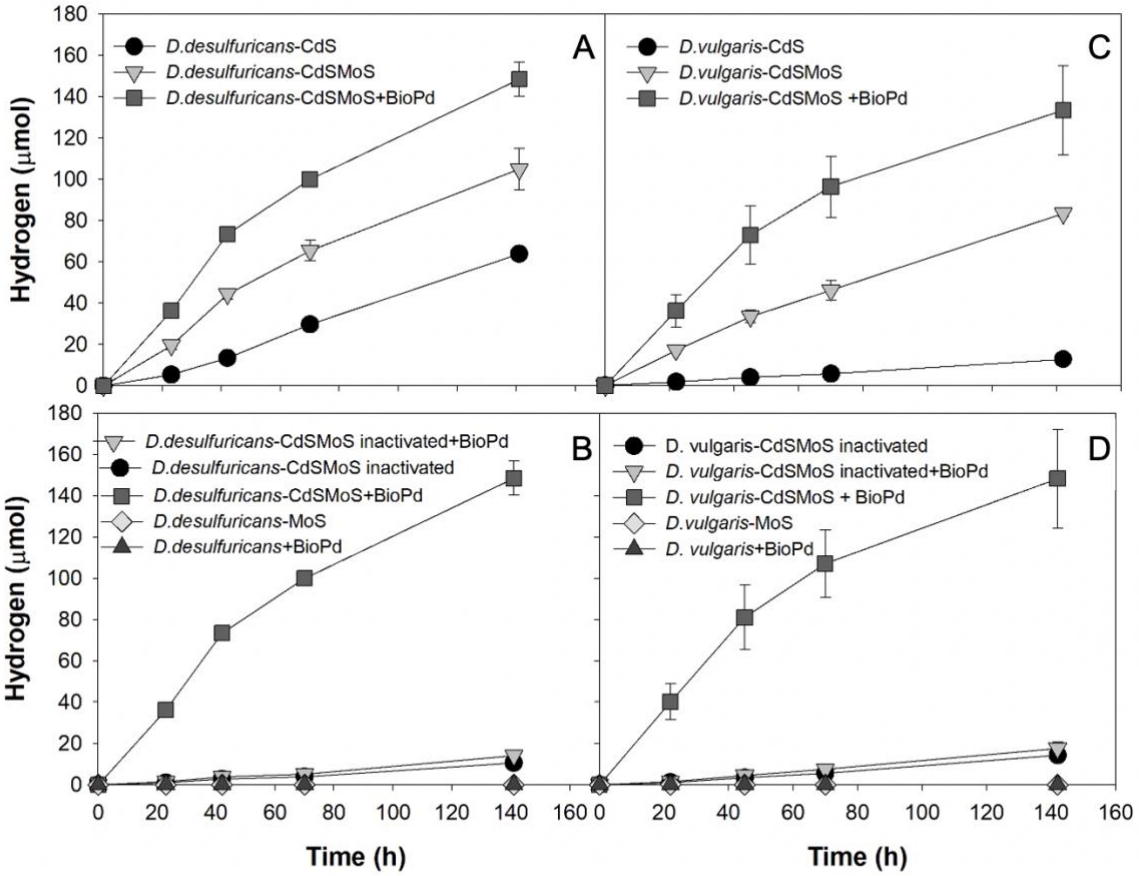

Figure 4.5: *Light-driven H_2 production profiles of different biohybrid systems constructed from D. desulfuricans (A and B) and D. vulgaris (C and D). Experiments were carried out in duplicate, data are shown as mean ± standard deviation.*

The data obtained in this study proved highly promising and provided greater yields when compared to other self-photosensitised biohybrid systems for the light-driven production of H_2. Previous work conducted by Martins et al. comparing the efficiencies of *C. freundii*-CdS, *S. oneidensis*-CdS, *E. coli*-CdS and *D. desulfuricans*-CdS had identified *D. desulfuricans*-CdS to be the most proficient biohybrid system in the production of solar biohydrogen in the absence of the electron shuttle, reaching a specific H_2 production rate of 36 µmol/g_{dcw}/h (114). In the optimised conditions in the presence of 81 mM of cysteine, the *D. desulfuricans*-CdS biohybrid system in this work was able to reach a specific H_2 production rate of 96 µmol /g_{dcw}/h and a quantum yield of 10% (Eq. 3) after 141 hours. The optimised *D. desulfuricans*-$CdSMoS_2$ + BioPd biohybrid system was able to improve on the results previously achieved even further by more than 8-fold, reaching a specific H_2 production rate of 299 µmol/g_{dcw}/h in the absence of an electron shuttle and reaching a quantum yield of 23% (Eq. 3) after 141 hours.*D. vulgaris*-$CdSMoS_2$ + BioPd equally achieved an AQY of 23% (Eq. 3) in the absence of MV, whereas the simple *D. vulgaris*-CdS biohybrid system only achieved an AQY of 2% (Eq. 3) after 142 hours.

Overall, the *Desulfovibrio* spp. assessed in this work appear very strong candidates for the light-driven H_2 production.

4.2 Light-driven CO_2 reduction assays

Besides H_2 production, CO_2 reduction was also investigated using the *Desulfovibrio*-CdS and *Desulfovibrio*-CdSMoS_2+BioPd biohybrids. The field of light-driven CO_2 reduction by *Desulfovibrio spp*. biohybrid systems is yet unexplored. Experiments were therefore conducted both in the presence and absence of the electron shuttle MV. Assays were conducted to determine the light-driven reduction of CO_2 into H_2 as well as the compounds formate and acetate.

4.2.1 Light-driven CO_2 reduction by different biohybrids in the presence of an electron shuttle

The *Desulfovibrio spp.* biohybrid systems in the presence of MV produced two products of interest sampled over the course of the assay, namely H_2, and the H_2 storage compound formate. The behaviour in the absence of MV is described in the next section.

After 24 hours, the *D. desulfuricans*-CdS biohybrid produced 10 ± 0 mM of formate (Fig. 4.6a), reaching a maximum formate production of 13 ± 2 mM after 70 hours, and 88 ± 14 µmol of H_2 (Fig. 4.6c). Similarly, the *D. vulgaris*-CdS biohybrid system was able to produce both H_2 as well as formate in response to light irradiation. Formate production slowly increased over 70 hours to reach a maximum of 7 ± 0 mM (Fig. 4.6b), whilst H_2 production peaked after 24 hours at 97 ± 7 µmol (Fig. 4.6d).
The early peak and subsequent decline of H_2 production is presumably due to the fact that cells are able to oxidise the H_2 originating electrons and protons that can be also used for the production of formate Therefore, it appears that the electron transfer to the hydrogenases might be faster than to the FDHs, explaining the early peak in H_2 production, however, in the presence of CO_2, the produced H_2 is subsequently consumed in the production of formate.
In contrast, the production of formate was fastest within the first 24 hours, but then either plateaued or slowly continued to increase (Fig. 4.6). This could be due to the formate dehydrogenases reaching their maximum velocity early on.

To test if the optimised conditions from the H_2 production assays would equally increase the efficiency of biohybrid systems for the reduction of CO_2, the *Desulfovibrio*-CdSMoS_2 + BioPd biohybrid systems

were assessed. In comparison to the simple biohybrid, the optimised *D. desulfuricans*-CdSMoS_2+BioPd biohybrid system produced 10 ± 0 mM of formate after 24 hours (Fig. 4.6a), equally reaching maximum formate concentration after 70 hours with 14 ± 1 mM, as well as 100 ± 4 µmol of H_2 (Fig. 4.6c). Although a substantial difference was observed in the assays for biological light-driven H_2 production, in the presence of MV this improvement of biohybrid performance was not observed in terms of CO_2 reduction and the results were within the same order of magnitude.

In comparison between species, formate production in the *D. vulgaris*-CdSMoS_2+BioPd biohybrid system was similar to the monovalent biohybrid system at 7 ± 0 mM after 70 hours (Fig. 4.6b), whereas it was able to reach a slightly higher maximum of 129 ± 9 µmol of H_2 after 22 hours (Fig. 4.6d). As with the *D. desulfuricans* biohybrids, it was observed once more that in the presence of the electron shuttle MV, light-driven CO_2 reduction was not much improved by the presence of MoS_2 and BioPd nanoparticles. As the main function of a co-catalyst is in facilitating the charge transfer from semiconductor to the microorganism (122), it appears that in the metabolic pathways leading to CO_2 reduction in the presence of an electron shuttle, these are either already more efficient, and therefore the presence of co-catalysts is neglible. Alternatively it is possible that at the given light intensity the production reached its possible maximum.

Inactivated controls were carried out by autoclaving the biohybrid systems prior to light irradiation. While the inactivated *D. desulfuricans*-CdS biohybrid did not produce H_2 nor formate, the inactivated *D. desulfuricans*-CdSMoS_2+BioPd biohybrid was able to produce small amounts of H_2, reaching 14 ± 1 µmol of H_2 after 70 hours (Fig. 4.6c). This suggests that the nanoparticles are able to catalyse a low level of H_2 production independently of the living cell in the presence of co-catalysts, however the main catalyst is the live *Desulfovibrio* enzymatic machinery. In the case of *D. vulgaris*, only the inactivated *D. vulgaris*-CdSMoS_2 + BioPd system produced a small amount of H_2, namely 17 ± 4 µmol after 65 hours (Fig. 4.6d), once again suggesting a small capability of independent catalytic activity of the nanoparticles in the presence of a semiconductor and co-catalyst, with the live cells being the main catalysts required for effective product formation.

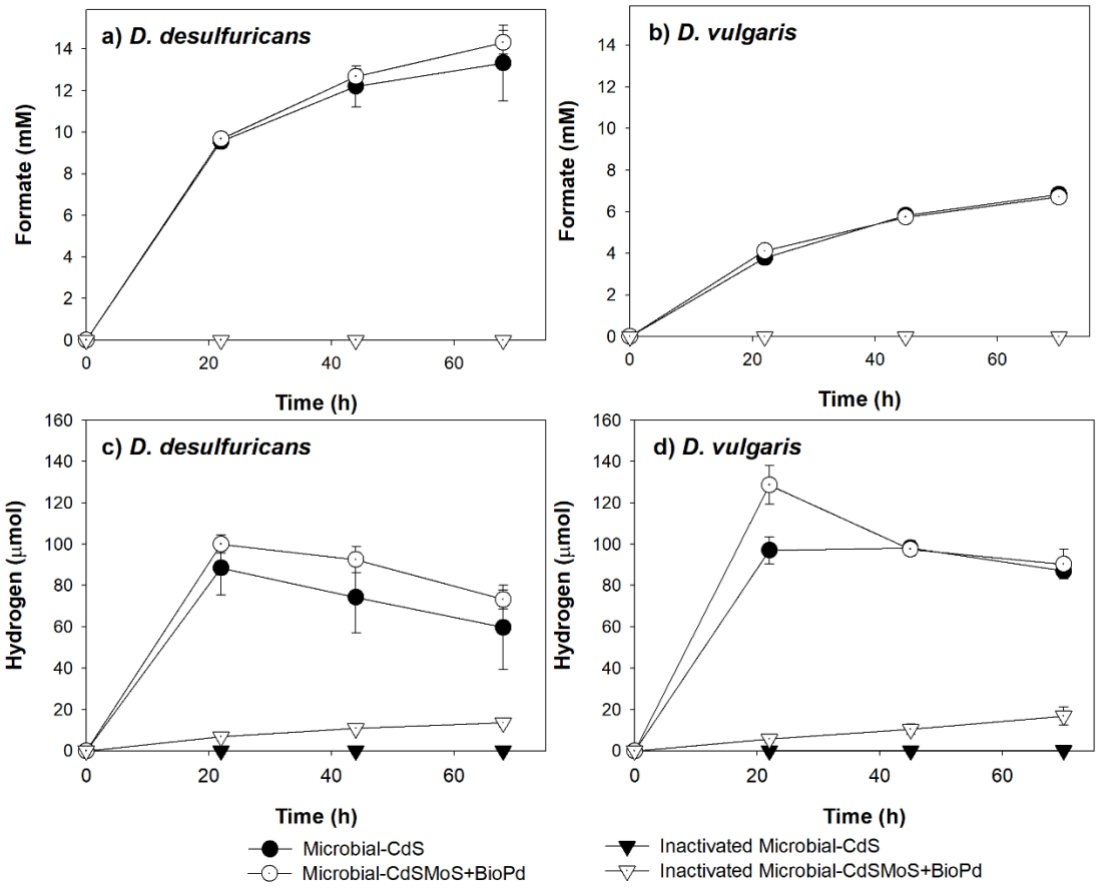

Figure 4.6: *Light-driven CO_2 reduction profiles of Desulfovibrio-CdS and Desulfovibrio-CdSMoS_2 + BioPd biohybrid systems in the presence of MV. The biohybrid systems were constructed with D. desulfuricans (a and c) as well as D. vulgaris Hildenborough (b and d). The production of formate (a and b) as well as H_2 (c and d) was observed. Experiments carried out in duplicate; data are shown as mean ± standard deviation.*

4.2.2 Light-driven CO_2 reduction by different biohybrid systems in the absence of an electron shuttle

The *D. desulfuricans*-CdS biohybrid in the absence of MV produced smaller quantities, but a wider variety of value-added compounds, reaching a maximum production of 3 ± 0 mM of formate after 68 hours (Fig. 4.7a) as well as 4 ± 1 µmol of H_2 after 22 hours (Fig. 4.7c) and 3 ± mM of acetate after 68 hours (Fig. 4.7e). The optimised biohybrid system of *D. desulfuricans*-CdSMoS_2+BioPd in the absence of MV performed much better than the monovalent biohybrid, reaching a maximum of 9 ± 2 mM of formate (Fig. 4.7a), 3 ± 0 µmol of H_2 (Fig. 4.7c) and 5 ± 0 mM of acetate (Fig. 4.7d) in the same time.

In the absence of MV, the monovalent *D. vulgaris*-CdS biohybrid system was much less efficient at value-added product formation than *D. desulfuricans*-CdS. After 68 hours, the peak of formate production was reached at 4 ± 0 mM (Fig. 4.7b), as well as H_2 at 5 ± 1 µmol (Fig. 4.7d). However, the

system was equally able to produce 1 ± 0 mM of acetate (Fig. 4.7f), which was not observed in the presence of the electron shuttle. The *D. vulgaris*-CdSMoS$_2$+BioPd composite biohybrid outperformed the single biohybrid, with 7 ± 1 mM of formate (Fig. 4.7b), 8 ± 0 µmol of H_2 (Fig. 4.7d) and 2 ± 0 mM of acetate produced after 68 hours (Fig. 4.7f).

As in the control experiments for the light-driven production of H_2 (section 4.2.4), the inactivated *Desulfovibrio*-CdSMoS$_2$+BioPd biohybrid was able to produce a small amount of H_2, which in the case of CO_2 reduction by the *D. desulfuricans*-CdSMoS$_2$ + BioPd biohybrid was even higher than that of the live biohybrid system. The inactivated *D. desulfuricans*-CdS biohybrid did not produce either H_2 nor organic compounds in the absence of MV, whereas the inactivated *D. desulfuricans*-CdSMoS$_2$+BioPd biohybrid, as in the presence of MV, was able to catalyse a low amount of H_2 production of 7 ± 1 µmol after 70 hours of irradiation (Fig. 4.7a, c, e). In the case of the inactivated controls for *D. vulgaris* biohybrid systems, once again only the composite inactivated biohybrid system with BioPd was able to produce 8 ± 0 µmol of H_2 after 68 hours (Fig. 4.7b, d, f).

This further confirms the hypothesis that nanoparticles in the presence of a co-catalyst are capable of low amounts of H_2 production, even when there is no more cellular viability. However, compared to the active *Desulfovibrio*-CdS and *Desulfovibrio*-CdSMoS$_2$+BioPd biohybrid, it appears the produced H_2 can not be used by the enzymatic machinery responsible for the conversion of CO_2, which could explain why the production remains higher than that of the live system.

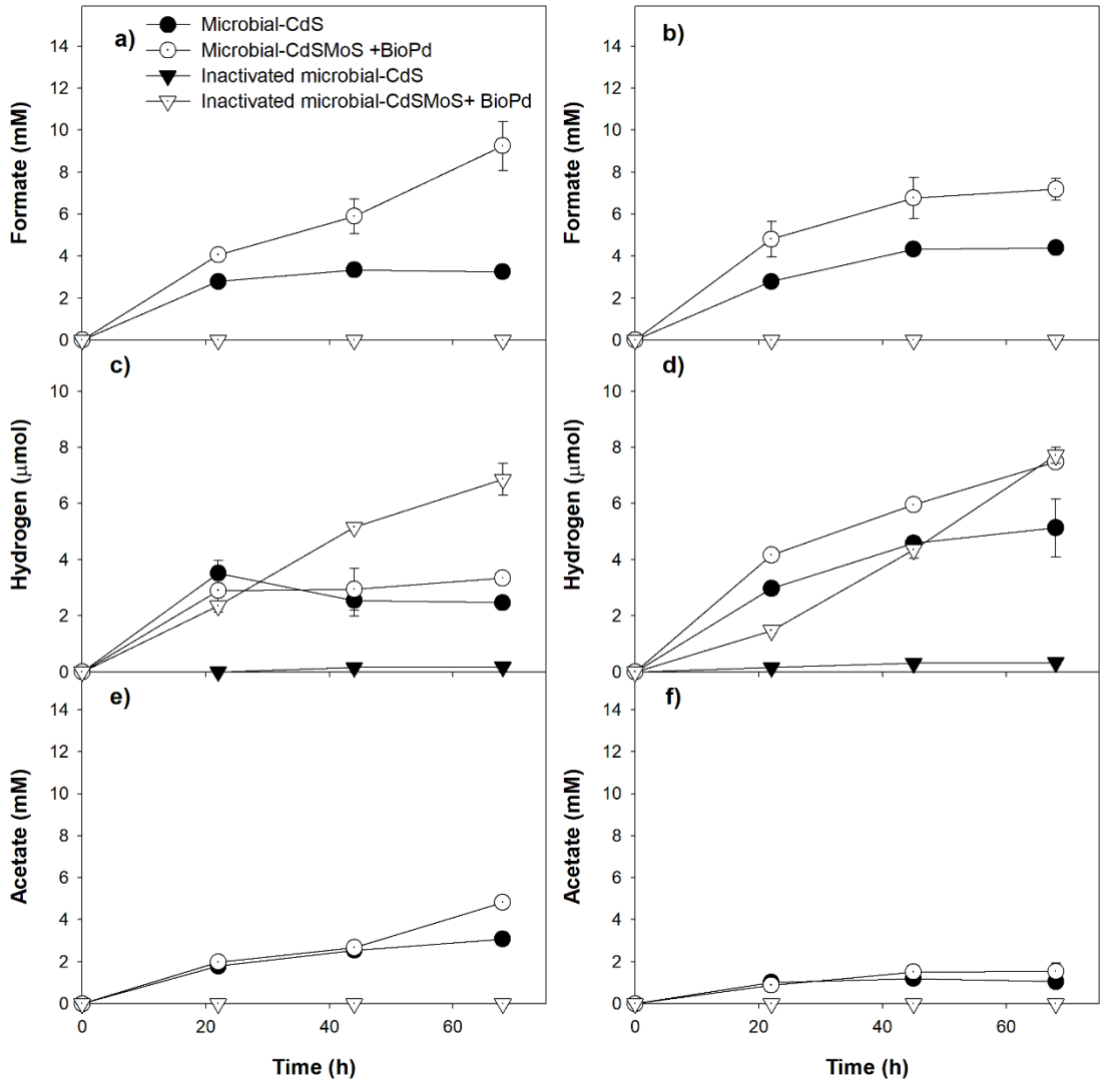

***Figure 4.7**: Light-driven CO_2 reduction profiles of Desulfovibrio-CdS and Desulfovibrio-CdSMoS$_2$ + BioPd biohybrid systems in the absence of MV. The biohybrid systems were constructed with D. desulfuricans (a, c and e) as well as D. vulgaris Hildenborough (b, d and f). The production of formate (a and b), H_2 (c and d) as well as acetate (e and f) was observed. Experiments carried out in duplicate, data are shown as mean ± standard deviation.*

Overall, the light-driven reduction of CO_2 by the biohybrids in the presence of the electron shuttle occurred at much faster rates and yielded more product, suggesting more efficient electron transfer kinetics into the cell. Interestingly, in both *D. desulfuricans* as well as *D. vulgaris* biohybrids, the difference between the simple *Desulfovibrio*-CdS-biohybrid and the composite *Desulfovibrio*-CdSMoS$_2$+BioPd was not as stark as that observed in the light-driven production of H_2, with the respective amounts of H_2 and formate produced being more or less in the same order of magnitude, irrespective of the presence of a co-catalyst (Table 4.1). There seems to be no advantage of using a co-catalyst with regards to both production rate and yield.

Between species there was however a noticeable difference, in that the *D. desulfuricans*-CdS and *D. desulfuricans*-$CdSMoS_2$ + BioPd produced about twice as much formate as the *D. vulgaris*-CdS and *D. vulgaris*-$CdSMoS_2$ + BioPd biohybrid systems. It appears once again that the electron transfer from semiconductor to the enzymatic machinery of *D. desulfuricans* is superior to that of *D. vulgaris* Hildenborough.

In the absence of the electron shuttle, biohybrid systems constructed with either species produced less formate as well as H_2, but in contrast to the assays in the presence of MV, acetate was produced, suggesting a different electron transfer pathway. Acetate has industrial use over wide ranging applications such as in cosmetics, cleaning materials and textiles. Without the electron shuttle present, there was also a bigger difference in the performance of the simple *Desulfovibrio*-CdS biohybrid system compared to the composite *Desulfovibrio*-$CdSMoS_2$ + BioPd biohybrid system. The light-driven reduction of CO_2 into value-added compounds by self-photosensitised biohybrid systems is still a burgeoning field of research in its initial stages. In their landmark study, Sakimoto et al. achieved the conversion of CO_2 into acetic acid, of which acetate is a conjugate base of, using the acetogenic *M. thermoacetica* for the construction of a *M. thermoacetica*-CdS biohybrid (104). Building up on those findings, Zhang et al. managed to further improve the performance of the *M. thermoacetica*-CdS biohybrid by replacing the extracellularly attached CdS nanoparticles with intracellularly ingested gold nanoclusters (AuNCs). This led to an improvement of the performance by 33% on the first day of irradiation with simulated sunlight and improved cellular viability, with an overall quantum yield of 2.86 ± 0.38% by *M. thermoacetica*–AuNCs compared with 2.44 ± 0.62% for the *M. thermoacetica*–CdS biohybrid (110). The biohybrid system constructed with the methanogenic *M. barkeri*-CdS biohybrid achieved the conversion of CO_2 into the alternative fuel methane (CH_4), with a production rate of 0.19 μmol/ h, and a quantum efficiency of 0.34% (133). Doping the CdS nanoparticles in a following study with Ni, the *M. barkeri*-Ni:CdS-biohybrid improved the CH_4 yield by about 250% and a QE of 2.08 % (131).

The AQY reached in the production of acetate of the *D. desulfuricans*-CdS and *D. vulgaris*-CdS biohybrid systems in this work reached 0,7% and 0,3% respectively after 68 hours (Eq. 3). In the monovalent biohybrid systems, the AQY was slightly higher, reaching 1% in the *D. desulfuricans*-CdSMoS2+BioPd and 0,4% in the *D. vulgaris*-CdSMoS2+BioPd biohybrid system respectively (Eq. 3).

To the best of my knowledge, this is the first study of a self-photosensitised biohybrid system showing successful conversion of CO_2 into the H_2 storage compound formate.

One of the major limiting factors of widespread H_2 use is the need for safe and efficient storage of a highly flammable compound. Improving applications leading to the production of formate therefore

prove important to explore. The biohybrid systems used in this work were successful in the production of formate. Formate production by the *D. desulfuricans*-CdS biohybrid system achieved an AQY of 3% and 1% after 70 hours in the presence and absence of MV respectively (Eq. 3). In the composite biohybrid system of *D. desulfuricans*-CdSMoS_2+BioPd, this came to an AQY of 3% and 2% respectively. In the *D.vulgaris*-CdS biohybrid system, formate production reached an AQY of 2% and 1% after 68 hours in the presence and absence of MV respectively (Eq. 3). In the *D. vulgaris*-CdSMoS_2 + BioPd biohybrid systems, 2% were achieved in both cases (Eq. 3).

Table 4.1: *Molar balance of light-driven CO_2 conversion into the different value-added products by the different Desulfovibrio-biohybrids.*

Biohybrid	**Production (µmol)[a)]**				**Consumption(µmol)[a)d)]**	
With MV	Formate	H_2[b)]	Acetate	Total	Cysteine	CO_2
D. desulfuricans-CdS	**87** ± 12	**89** ± 13	n.d. [c)]	**176** ± 25	**351** ± 50	**87** ± 12
D. desulfuricans-CdSMoS_2+BioPd	**93** ± 4	**100** ± 4	n.d. [c)]	**193** ± 8	**386** ± 16	**93** ± 4
D. vulgaris-CdS	**44** ± 2	**98** ± 4	n.d. [c)]	**140** ± 6	**280** ± 12	**44** ± 2
D. vulgaris-CdSMoS_2+BioPd	**44** ± 2	**129** ± 9	n.d. [c)]	**173** ± 11	**346** ± 22	**44** ± 2
Without MV	Formate	H_2	Acetate	Total	Cysteine	CO_2
D. desulfuricans-CdS	**21** ± 2	**4** ± 1	**20** ± 0	**45** ± 3	**209** ± 8	**61** ± 3
D. desulfuricans-CdSMoS_2+BioPd	**60** ± 8	**3** ± 0	**31** ± 1	**94** ± 9	**375** ± 24	**122** ± 10
D. vulgaris-CdS	**29** ± 0	**5** ± 1	**8** ± 0	**42** ± 1	**130** ± 2	**45** ± 0
D. vulgaris-CdSMoS_2+BioPd	**47** ± 3	**8** ± 0	**10** ± 3	**65** ± 6	**189** ± 27	**67** ± 8

[a)] Production and consumption obtained after 68 h of light irradiation.
[b)] Maximum H_2 accumulated after 22h of light irradiation in the presence of MV before declining.
[c)] Not detected
[d)] Values calculated according with the stoichiometry of reactions involved.

4.3 Biohybrid system production and characterisation

The biohybrid systems were generated through cell growth in the presence of sulfate, followed by incubation with $CdCl_2$ (and Na_2MoO_4 where applicable). Successful synthesis of the biohybrid system was observed through the formation of a yellow colour following $CdCl_2$ addition, indicating the formation of CdS as a result of the precipitation with metabolically produced H_2S. In the case of biohybrids incubated with Mo, the observed colour was slightly more orange. This is presumably due to molybdenum disulfide (MoS_2) having a natural brown colour (134), therefore turning the suspension with the yellow of the CdS more orange.

4.3.1 Characterisation of the *Desulfovibrio*-CdS-MoS_2 biohybrid by SEM-EDS and TEM-EDS

Characterisation of the *D. desulfuricans*-CdS-biohybrid system was previously described by Martins et al. to show evenly distributed CdS clusters across the bacterial membrane (114). Following on from Martins et al.'s work, in this work the novel biohybrid systems of *D. desulfuricans* with the use of co-catalysts were characterised, as well as the systems based on *D. vulgaris* Hildenborough. The *Desulfovibrio*-$CdSMoS_2$ and *Desulfovibrio*-$CdSMoS_2$ + BioPd biohybrids were characterised by SEM and SEM-EDS as well as TEM and TEM-EDS. SEM images of the *D. desulfuricans*-$CdSMoS_2$-biohybrid showed a high density and even distribution of precipitated $CdSMoS_2$ nanoparticles on the cell surface (Fig. 4.8A). These were ranging in size from smaller clusters to larger aggregates as shown by TEM (Fig. 4.8B and C). Similarly, in the *D. vulgaris*-$CdSMoS_2$ biohybrid, nanoparticle clusters were distributed across the cell surface, but there was a greater variation observed by SEM between cells with and cells without precipitated nanoparticles (Fig. 4.8D). TEM analysis showed fewer clusters per cell of smaller size than when compared with the *D. desulfuricans*-$CdSMoS_2$ biohybrid (Fig. 4.8E). SEM-EDS analysis confirmed the composition of the nanoparticles to be cadmium, sulfur and molybdenum. Osmium, which was used in the preparation of the sample, was equally detected (Fig. 4.8G).

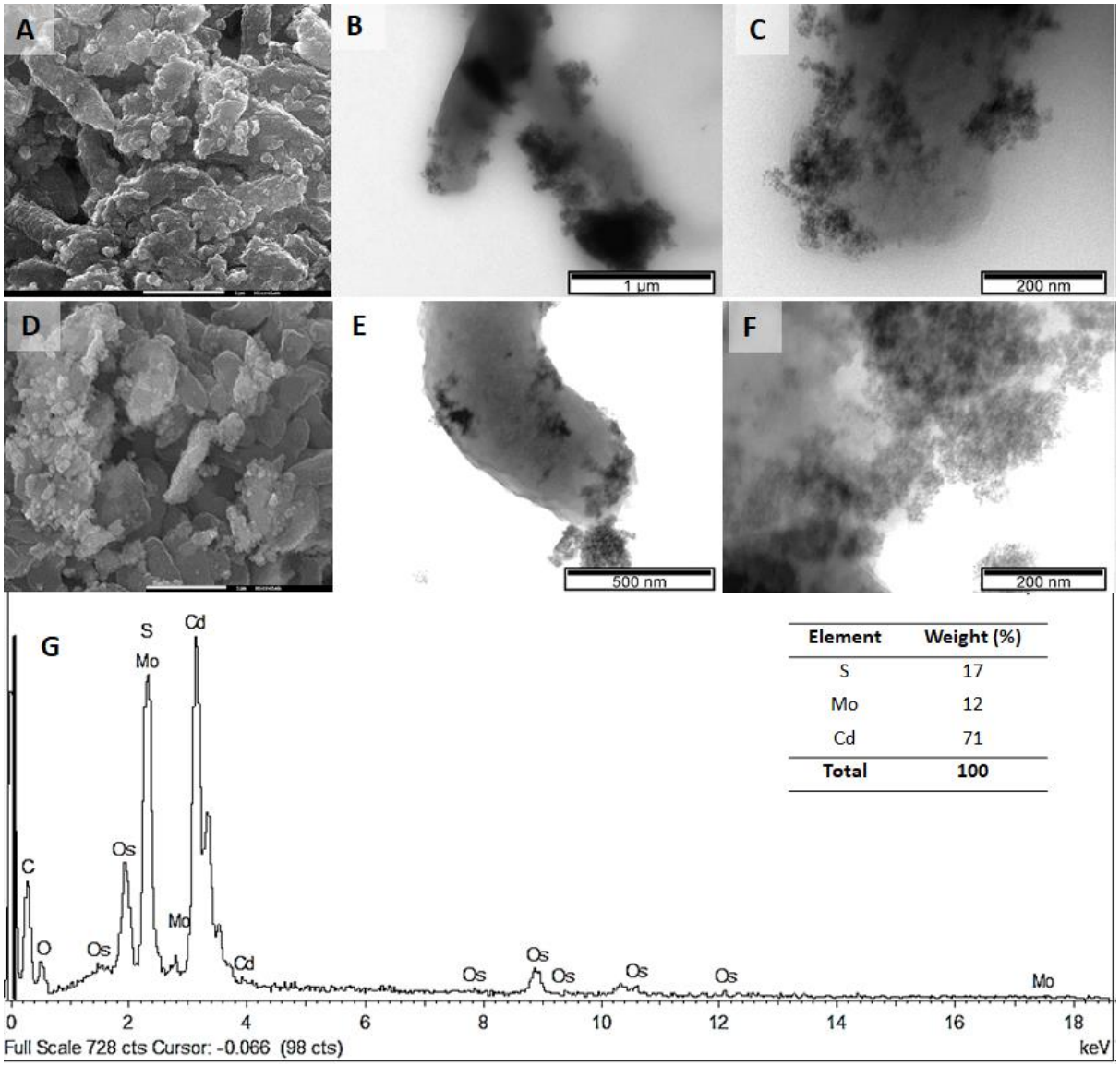

Figure 4.8: *Characterisation of the Desulfovibrio-CdSMoS2 biohybrids. SEM analysis of D. desulfuricans-CdSMoS2 (A) and D. vulgaris-CdSMoS2 (D) biohybrids at 1 µm scale. TEM analysis of D. desulfuricans-CdSMoS2 (B and C) and D. vulgaris-CdSMoS2 (E and F) biohybrids. Representative SEM-EDS analysis of D. desulfuricans-CdSMoS$_2$ biohybrid (G)*

In the previous characterisation of the *D. desulfuricans*-CdS biohybrid system by Martins et al., the authors reported a high densitiy of self-precipitated CdS nanoparticles on the surface of the bacterium, confirmed to be consisting of cadmium and sulfur by both SEM-EDS and XRD. Aside from the clusters attached to the cell, they observed a few extracellular clusters (114). The *Desulfovibrio*-CdSMoS$_2$ biohybrid systems analysed in this work equally show the clusters to be mainly attached to the cells, suggesting that MoS$_2$ colocalises with CdS during the initial step of precipitation. In the work by Wang et al on the self-photosensitised *E. coli*-CdS biohybrid system, the observed nanoparticles precipitated across the bacterial membrane and periplasmic space were ranging from about 15-20 nm in size and of high uniformity (106). The nanoparticles created in the E. coli AgInS$_2$

/InS_3 equally showed a size of about 15-20 nm, and where predominantly spread across the periplasm (107). Self-photosensitisation was also achieved in electro active microbes with CdS, showing spherical CdS structures on the cell membrane of approximately 50-100 nm (135). In this work, the nanoparticles appeared in clusters rather than independently, making it hard to determine their individual size.

4.3.2 Characterisation of the *Desulfovibrio* spp. biogenic palladium nanoparticles by SEM-EDS and TEM-EDS

Previous experiments showed an improvement in the performance of chemically synthesised semiconductors if these were loaded with metals from the platinum metal group (123). For the purpose of this work, palladium nanoparticles were biologically synthesised (denominated BioPd). Both microorganisms used in this study, *D. desulfuricans* and *D. vulgaris* Hildenborough were able to biologically synthesise palladium nanoparticles. SEM images of BioPd nanoparticles synthesised by *D. desulfuricans* showed small, highly dense and evenly distributed Pd clusters on the cell surface (Fig. 4.9A). SEM images of BioPd nanoparticles synthesised by *D. vulgaris* showed more diverse clusters of Pd, that were generally slightly larger than the ones observed in *D. desulfuricans*, but also fewer and farther between, with some large clusters (Fig. 4.9D).

TEM images captured the presence of larger palladium aggregates of nanoparticles on the cell surface in *D. desulfuricans* BioPd, with the aggregates ranging from 200-500 nm in size, interspersed with many smaller ones (Fig. 4.9B and C). In comparison, *D. vulgaris* BioPd cell aggregates captured on individual cells were much smaller compared with *D. desulfuricans*, of approximately 50-100 nm in size (Fig. 4.9E and F). SEM-EDS confirmed the presence of palladium (Fig. 4.9G).

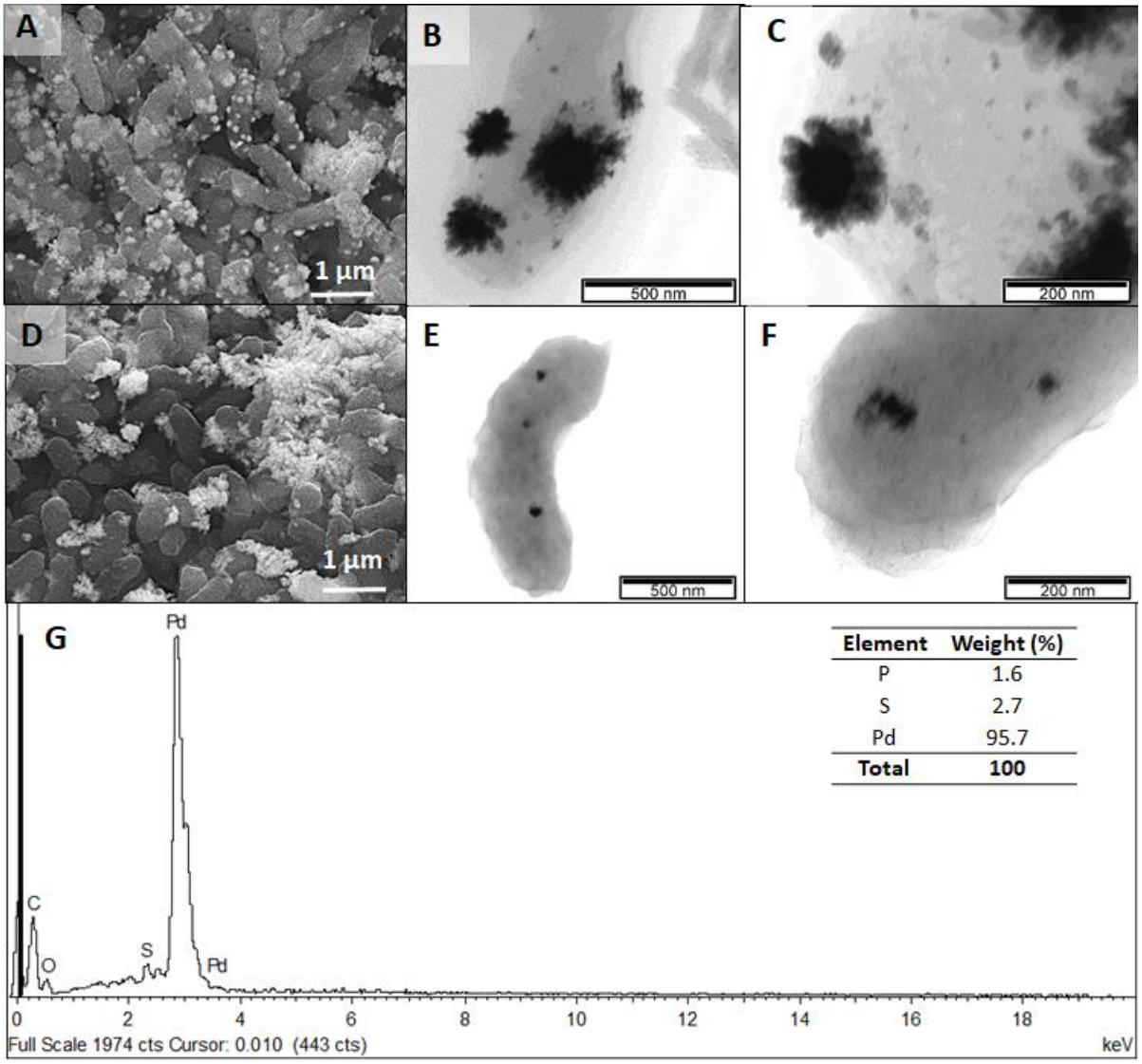

Figure 4.9: *Characterisation of the Desulfuvobrio palladium nanoparticles. SEM analysis of BioPd synthesised by D. desulfuricans (A) and D. vulgaris (D). TEM analysis of BioPd synthesised by D. desulfuricans (B and C) and D. vulgaris (E and F). Representative SEM-EDS analysis of BioPd (G).*

Martins et al. previously constructed BioPd nanoparticles using *D. vulgaris* Hildenborough for the biocatalytic removal of pharmaceuticals (117). They observed dense metal precipitates with the largest ones just up to 100 nm in size across the surface of the bacterium as well as in the periplasmic space. In a study by Capeness et al., palladium nanoparticles were created and shown to attach to the cells using the SRB *Desulfovibrio alaskensis* G20. In their representative TEM electron micrograph showing two cells, the distribution of Pd across the cells was very different, one of them exhibiting a high number of palladium nanoparticle aggregates of up to 400 nm big, and the neighbouring cell showing very few (136). This uneven distribution was equally observed in the nanoparticles created by *D. vulgaris* Hildenborough in this work, whereas the distribution across *D. desulfuricans* appeared more even.

Palladium nanoparticles using *D. desulfuricans* were equally constructed in a study by Wu et al. in 2010 using lactate as the electron donor. The observed particles were observed as dark spots distributed across the cell membrane with different shapes and sizes of an average of 10 nm (137).
The biogenic synthesis of nanomaterials is a cost-effective and more environmentally friendly alternative to chemical synthesis, as it does not require the use of toxic chemicals or energy intensive production processes (138). As metals from the platinum group are fairly rare and expensive, if it can be achieved, the coupling of biogenic nanoparticle creation through bioremediation processes to the creation of alternative energy sources such as proposed in this work would be an excellent way of contributing to a circular and sustainable economy.

4.3.3 Characterisation of the *Desulfovibrio*-$CdSMoS_2$ + BioPd biohybrid system by SEM-EDS and TEM-EDS

In order to optimise the performance of the *Desulfovibrio*-$CdSMoS_2$ biohybrid, BioPd nanoparticles were added to biohybrid systems in order to construct new multivalent *Desulfovibrio*-$CdSMoS_2$ + BioPd biohybrid systems.

The images obtained show the presence of the CdS nanoparticles precipitated on the cell surface of the bacteria in the *Desulfovibrio*-$CdSMoS_2$+BioPd biohybrid system (Fig. 4.10A-D). SEM-EDS mapping for both biohybrid systems showed the distribution of Pd, cadmium (Cd), sulfur (S) and molybdenum (Mo) in both of the *Desulfovibrio*-$CdSMoS_2$+BioPd biohybrid systems (Fig. 4.10G-I for *D. desulfuricans* and L-N for *D. vulgaris*). The same distribution on the cells was observed for S, Cd and Mo, which agrees with the precipitation of Cd as CdS and Mo as MoS_2. Moreover, this also indicates that the CdS and MoS_2 are jointly distributed. A different behaviour was observed with Pd. The SEM-EDS mapping showed that the Pd nanoparticles are concentrated in some cells. These results can be explained by the fact that Cd and Mo are introduced at same time during the initial biohybrid formation, thus leading to the simultaneous precipitation of Cd and Mo as CdS and MoS_2 with the H_2S produced by the cells. On the other hand, BioPd was synthetised separately and mixed with the CdS-MoS_2 biohybrids, leading to the concentration of Pd in different locations (Figure 10F and K).

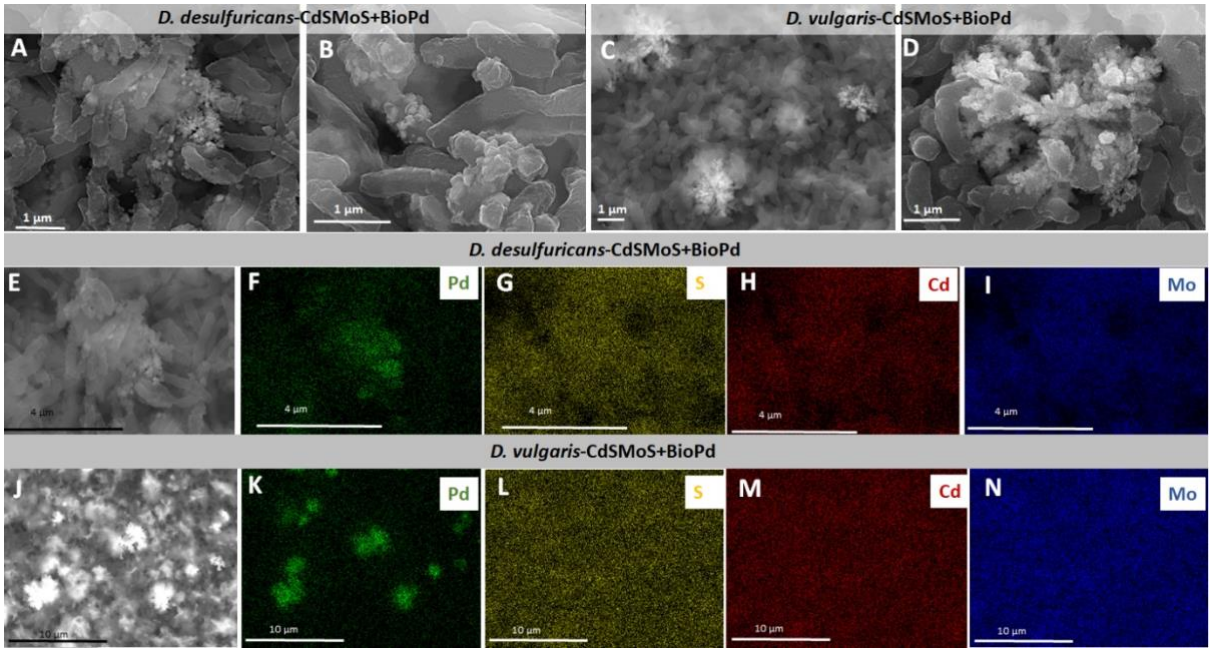

Figure 4.10: *SEM Mapping of Desulfovibrio-CdSMoS2+ BioPd biohybrids.D. desulfuricans-CdSMoS2+BioPd (A, B, E-I) and D. vulgaris-CdSMoS2+BioPd (C, D, J-N).*

4.4 Evaluation of the role of hydrogenases and formate dehydrogenases in the photocatalytic bioprocesses

An important factor for future optimisation of photocatalytic bioprocesses is a deeper understanding of the enzymatic machinery involved in the processes for both H_2 production as well as CO_2 reduction. A deeper understanding of the mechanisms underlying the production will allow for targeted genetic manipulation and thus an increase in the system efficiency beyond the simple optimisation of conditions.

As *D. vulgaris* Hildenborough is genetically modifiable (139,140), assays were carried out in *D. vulgaris* to allow for a potential future base for targeted gene editing. All assays were carried out under the previously established optimal conditions of the composite *D. vulgaris*-$CdSMoS_2$+BioPd – biohybrid system.

4.4.1 Role of Hys hydrogenase in Light-Driven H_2 production by *D. vulgaris*-biohybrid

Across *Desulfovibrio* species, there is a large versatility of H_2 metabolism and a complex hydrogenase system, comprised of several expressed enzymes of both the [NiFe] and [FeFe]-hydrogenase types, with varying cellular localisation and subunit composition (141,142). The genome of *D. vulgaris* Hildenborough encodes seven different hydrogenases, of which four are located in the periplasm and three in the cytoplasm or facing the latter (Fig. 4.11). The periplasmic hydrogenases include the [NiFeSe]-hydrogenase Hys, the [FeFe]- hydrogenase Hyd and the two [NiFe]-hydrogenases HynAB-1 and HynAB-2. Facing the cytoplasm are the two hydrogenases Ech and Coo, which are both membrane-associated energy-conserving hydrogenases. Finally, found soluble within the cytoplasm is a [FeFe]-hydrogenase(142). To gain more insight into the enzymes involved, assays for the light-driven H_2 production with the *D. vulgaris*-$CdSMoS_2$+BioPd biohybrid systems using genetically engineered strains were conducted. H_2 production of a deletion mutant of the Hys hydrogenase (Δ*Hys*) was compared with the wildtype strain in the absence of an electron shuttle. The presence of Selenium (Se) in the growth medium leads to the [NiFeSe] hydrogenase being majorly expressed, as both the [NiFe] and [FeFe]-hydrogenases are downregulated as a result (143). Therefore, this mutant was selected to investigate the role of the [NiFeSe]-hydrogenase in light-driven H_2 production in *D. vulgaris* Hildenborough.

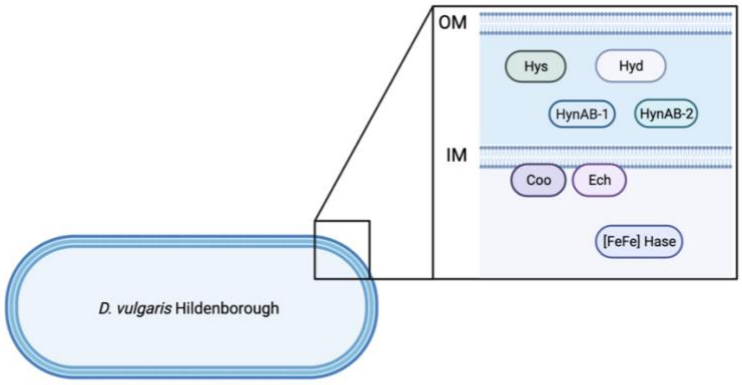

Figure 4.11*: Schematic representation of the cellular localisation of the seven hydrogenases encoded in the D. vulgaris Hildenborough genome. IM = inner membrane, OM = outer membrane. Created with BioRender.com*

Interestingly, the deletion did not significantly affect overall H_2 production, with the wild type producing 135 ± 15 µmol after 142 hours and the *ΔHys* mutant producing a slightly lower 113 ± 1 µmol (Fig. 4.12). Although the growth medium is supplemented with Ni, Se and Fe, making Hys the assumed

predominant hydrogenase in the biohybrid system, the deletion did not greatly affect the specific production of H_2. This is most likely due to electrons being redirected to the [NiFe] and [FeFe] Hases, which are able to compensate for the deletion.

As the [NiFeSe] hydrogenase is periplasmic, the electron transfer in its absence would be expected to favour the other periplasmic hydrogenases, namely Hyd, HynAB-1 and HynAB-2. However, it might be possible that in the absence of the predominant [NiFeSe] Hase in the periplasm, more electrons are transferred to the cytoplasmic or cytoplasm-facing hydrogenases Ech and Coo or the soluble [FeFe]-hydrogenase.

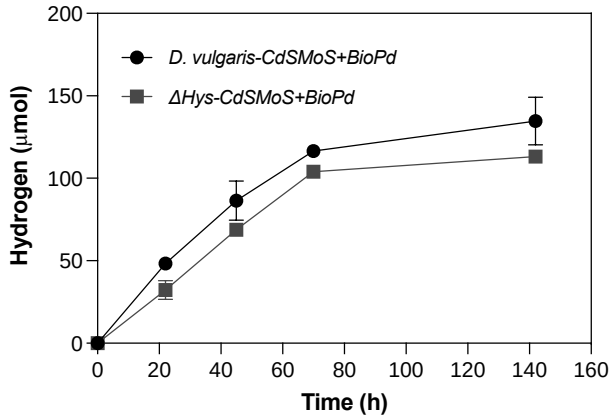

Figure 4.12: *Light-driven H_2 production profiles by different D. vulgaris-CdSMoS$_2$+BioPd biohybrids in the absence of an electron shuttle. Comparison between the wild type and Hys deletion mutant (ΔHys). Experiments were carried out in duplicate; data are shown as mean ± standard deviation.*

4.4.2 Role of FdhAB on the Light-Driven CO_2 reduction by *D. vulgaris*-biohybrid in the presence of an electron shuttle

The genome of *D. vulgaris* Hildenborough encodes three FDHs, of which two are soluble and periplasmic, namely FdhAB and FdhABC$_3$, as well as a periplasmic but membrane-bound third FdhM (115) (Fig. 4.13).

Previous work had shown that of the two predominantly expressed FDHs, FdhAB and FdhABC$_3$, expression levels were regulated by the presence of co-factors in the growth medium. FdhABC$_3$ becomes the main expressed enzyme in the presence of Mo. In the presence of W however, FdhAB is upregulated (144). Whilst FDHs are responsible for the oxidation of formate to CO_2, under syntrophic conditions (absence of electron acceptor) they can act as CO_2-reductases as well, producing formate from CO_2 and H_2 instead. In the absence of sulfate, FdhAB was shown to be the main FDH responsible for formate production from CO_2 (115) and is the subject of the following work. The function of the

FdhAB mutant was investigated by comparing the CO_2 reduction performance of the wild type strain with a FdhAB deletion mutant (Δ*FdhAB*) (115) as well as a FdhAB overexpressing strain containing a recombinant plasmid leading to 3x higher production than the wild type (83).

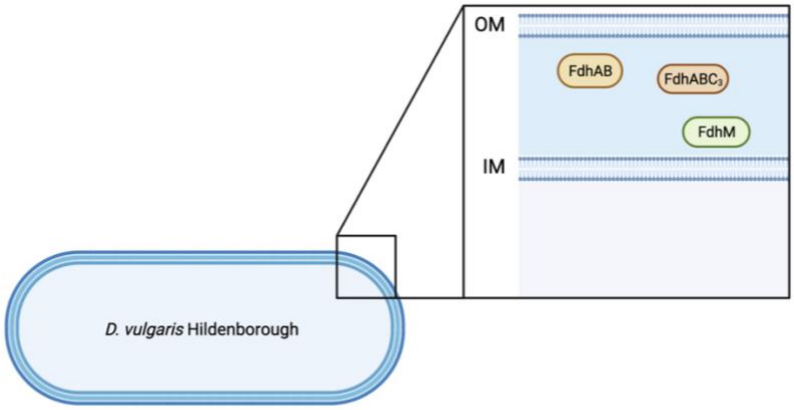

Figure 4.13: *Schematic representation of the cellular localisation of three periplasmic FDHs encoded in the D. vulgaris Hildenborough genome. IM = inner membrane, OM = outer membrane. Created with BioRender.com*

The Δ*FdhAB*-CdSMoS$_2$+BioPd-biohybrid achieved a production of formate that was approximately ½ the amount in comparison to the wild type, with 4 ± 0 mM vs 10 ± 0 mM produced respectively (Fig. 4.14a). Furthermore, it produced more H_2 (145 ± 5.4 µmol) than the wild type (114 ± 1.3 µmol) (Fig. 4.14b).

This makes sense as this is expected to be the main FDH to be expressed in this growth media and the produced H_2 would not be used for formate production. No other organic compounds were produced. The recombinant Rec*FdhAB*-CdSMoS$_2$+BioPd-biohybrid system produced a maximum of 18 ± 1 mM of formate after just 46 hours (Fig. 4.14a). In addition, less H_2 was produced than both other systems, at 64 ± 9 µmol (Fig. 4.14b), which can be explained by the electrons being more efficiently transmitted to the more abundant FDHs, reflected in the vast improvement of formate production. The production of formate in the Rec*FdhAB*-CdSMoS$_2$+BioPd-biohybrid occurred at a very fast rate during the first 22 hours, already producing 17 mM of formate at an AQY of 13% (Eq. 3) after which it plateaued (Fig. 4.14a). This could potentially be due to the FDH enzymes reaching their maximum velocity and turnover.

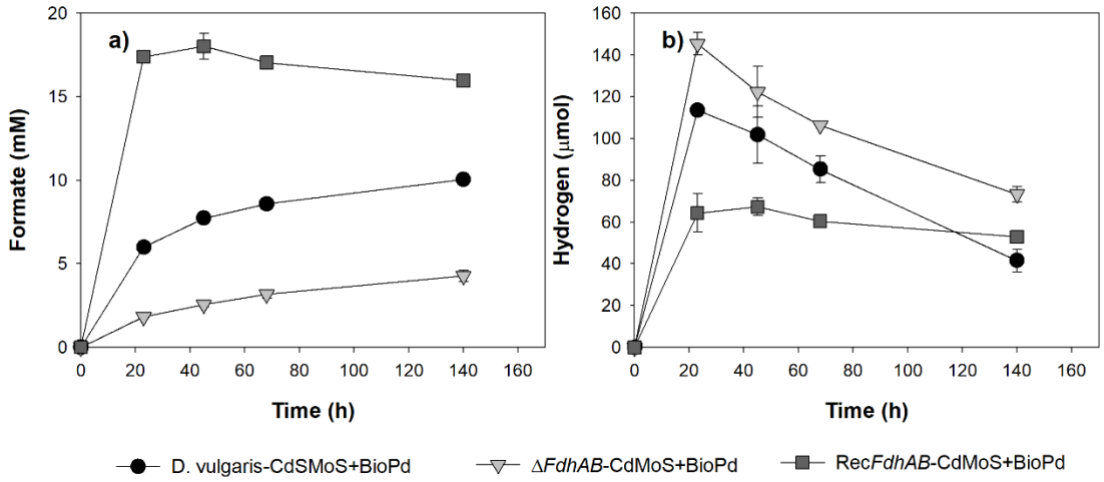

***Figure 4.14**: Light-driven CO_2 reduction profiles by different D. vulgaris-CdSMoS$_2$+BioPd biohybrids in the presence of an electron shuttle into value-added products formate (a) and H_2 (b). Comparison between the wild type, FdhAB deletion mutant (ΔFdhAB) and FdhAB overexpressing recombinant strain (RecFdhAB). Experiments were carried out in duplicate; data are shown as mean ± standard deviation.*

4.4.3 Role of FdhAB on light-driven CO_2 reduction by *D. vulgaris*-biohybrid in the absence of an electron shuttle

In the absence of MV, a variety of different organic compounds being produced were observed, suggesting a different pathway of the photoexcited electrons within the cell.

Formate production in the Δ*FdhAB*-CdSMoS$_2$+BioPd biohybrid system was lower at 4 ± 0 mM in comparison to 11 ± 0 mM produced by the wild type (Fig. 4.15a). The Δ*FdhAB*-CdSMoS$_2$+BioPd also produced more H_2 than the wild type, with 32 ± 4 µmol and 19 ± 5 µmol produced respectively (Fig. 4.15b), presumably once again due to an increased availability of photoexcited electrons being transferred to the Hases and fewer to the FDHs. With regards to acetate production, there was no difference observed, with both strains producing 2 ± 0 mM of acetate (Fig. 4.15c).

The Rec*FdhAB*-CdSMoS$_2$+BioPd-biohybrid produced slightly more formate as well as H_2 in comparison to the wild type, producing 13 ± 0 mM of formate (Fig. 4.15a), 24 ± 1 µmol of H_2 (Fig 4.15b) and 1 ± 0 mM of acetate (Fig 4.15c), however the improvement was not as stark as that observed in the presence of MV.

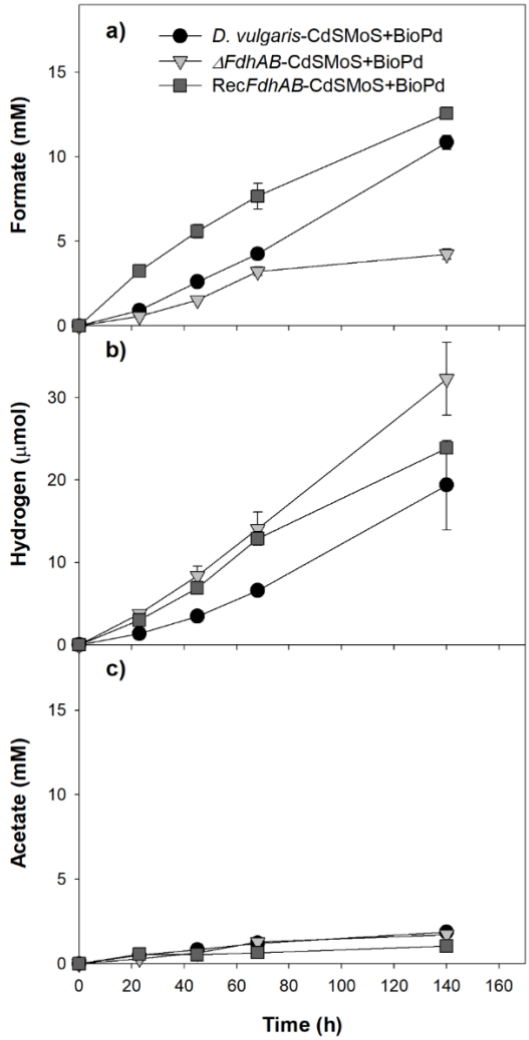

Figure 4.15*: *Light-driven CO_2 reduction profiles by different D. vulgaris-CdSMoS$_2$+BioPd biohybrids in the absence of an electron shuttle into value-added products formate (a), H_2 (b) and acetate (c). Comparison between the wild type, FdhAB deletion mutant (ΔFdhAB) and FdhAB overexpressing recombinant strain (Rec*FdhAB*). Experiments were carried out in duplicate; data are shown as mean ± standard deviation.

4.4.4 Summary of the function of FDHs for the light-driven CO_2 reduction by different *D. vulgaris* biohybrid systems

As in the previous light-driven CO_2 reduction assays, even the mutant strains did not produce acetate in the presence of MV. The Δ*FdhAB*-CdSMoS$_2$+BioPd having a much reduced formate production in comparison to the wild type reinforces the predominant role of FdhAB in the production of formate from CO_2 in growth media with W. As expected, the *RecFdhAB*-CdSMoS$_2$+BioPd had a much higher production of formate compared to the wild type, however this was not 3x as high, which would equate to the expression levels of the enzyme, reaching a very high AQY of 13% after just 22 hours (Eq. 3), therefore being very successful. Interestingly, in the absence of the electron shuttle, the situation is

slightly different. Whilst the Δ*FdhAB*-CdSMoS$_2$+BioPd once again performed poorly with regards to formate production, the difference between the wild type and recombinant strain was not as stark, with production of formate, H_2 and acetate all falling within the same order of magnitude (Table 4.2). It is possible that at lower electron transfer kinetics, such as in the absence of an electron shuttle, the transfer to the FDHs is not as efficient, and so even though the Δ*FdhAB*-CdSMoS$_2$+BioPd has a higher expression level, some of the photoexcited electrons may be "lost" to other cellular processes. Furthermore, the light intensity could be a limiting factor.

Table 4.2: *Molar balance of light-driven CO_2 conversion into the different value-added products by mutant strains of the D. vulgaris-biohybrids.*

Biohybrid	**Production (µmol)[a)]**				**Consumption (µmol)[a)d)]**	
With MV	Formate	H_2[b)]	Acetate	Total	Cysteine	CO_2
D. vulgaris-CdSMoS$_2$+BioPd	**65** ± 1	**114** ± 1	n.d. [c)]	**179** ± 2	**358** ± 4	**65** ± 1
Δ*FdhAB*-CdSMoS$_2$+BioPd	**28** ± 2	**145** ± 5	n.d. [c)]	**173** ± 8	**346** ± 16	**28** ± 2
RecFdhAB-CdSMoS$_2$+BioPd	**117** ± 5	**64** ± 9	n.d. [c)]	**181** ± 14	**362** ± 28	**117** ± 5
Without MV	Formate	H_2	Acetate	Total	Cysteine	CO_2
D. vulgaris-CdSMoS$_2$+BioPd	**70** ± 3	**19** ± 5	**12** ± 0	**89** ± 8	**274** ± 17	**94** ± 3
Δ*FdhAB*-CdSMoS$_2$+BioPd	**28** ± 2	**32** ± 4	**11** ± 0	**60** ± 7	**208** ± 16	**50** ± 3
RecFdhAB-CdSMoS$_2$+BioPd	**82** ± 2	**24** ± 1	**7** ± 0	**106** ± 3	**268** ± 8	**96** ± 3

[a)] Production and consumption obtained after 142 h of light irradiation.
[b)] Maximum H_2 accumulated after 22h of light irradiation in the presence of MV before declining.
[c)] Not detected
[d)] Values calculated according with the stoichiometry of reactions involved.

4.5 Development of a photobioreactor for the light-driven production of hydrogen

An important aspect for any alternative fuel with the serious aim of being able to replace fossil fuels is the need for scale up to huge levels in order to meet the ever-increasing global energy demand. To test the potential scalability of the systems created, a bench-scale photobioreactor was created.

In order to set up the development of a bioprocess for the light-driven production of H_2, a column bioreactor was tested using the *D. vulgaris*-CdSMoS$_2$+BioPd-biohybrid as a catalyst. The biohybrid was chosen due to its genetic tractability and therefore greater potential for genetic manipulation further along the line. The photobioreactor was constructed in an exact scale up of the system, increasing the working volume from 6.5 ml to 400 ml and in the absence of the electron shuttle MV and 81 mM of cysteine.

After 42 hours, the reactor reached a maximum production of 10 mmol of H_2 (Fig. 4.16), a stark increase in comparison to the smaller working volume, which was only able to produce 0.07 mmol after 45 hours and a maximum of 0.14 mmol after 142 hours. This increase is higher than that expected just from the increase in volume indicating a more efficient use of light.

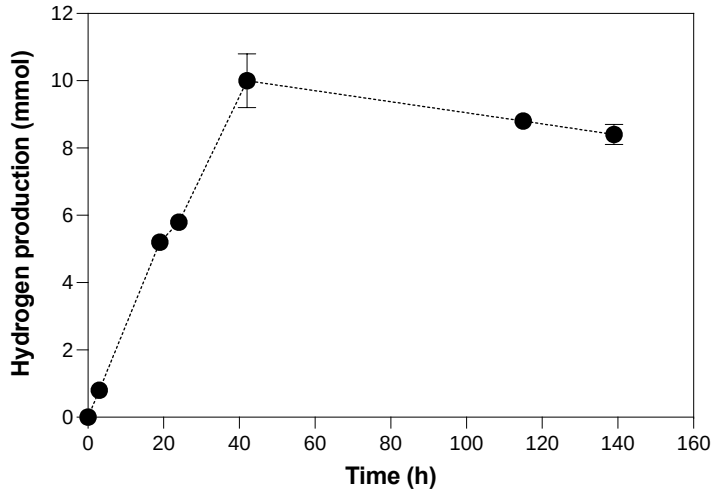

Figure 4.16: *Light-driven H_2 production profile by D. vulgaris-$CdSMoS_2$+ BioPd in a batch mode column photobioreactor with a light intensity of 2 Wm^{-2}.*

The scale up was highly successful and provides a huge improvement on the production of H_2 by a biohybrid system. As the concentration of the SED was 81 mM, this means that a theoretical maximum of 40.5 mM of H_2 can be produced. In a working volume of 400 ml, that equates to 32.4 mmol of cysteine and a maximum of 16.2 mmol of H_2 (Eq. 7).

0.081 mol / l
0.0081 mol / 100 ml
0.0324 mol / 400 ml (Equation 7)

The photobioreactor was able to produce 10 mmol of H_2 after only 42 hours, meaning 63% of the cysteine was converted in the absence of an electron shuttle, therefore proving extremely successful. As cysteine does not only act as SED but also functions as a reducing agent (145), it is possible that some of the cysteine was consumed in the reduction of oxygen (O_2) present in the reactor. This could explain, together with the fact that in the absence of an electron shuttle it is unlikely to reach maximum H_2 production, the stabilisation of the system after 42 hours.

5 Conclusion

Whilst we still have a long way to go before any technology can seriously be viewed as a viable competitor to fossil fuels, one can be optimistic as to the development of current and emerging technologies for the conversion of sunlight into energy. The results in this thesis provide a promising starting point for future research to be conducted on the use of semi-artificial biohybrid systems in the shift towards a decarbonised energy sector and the use of clean and sustainable fuels. The *Desulfovibrio*-CdSMoS$_2$+BioPd biohybrid systems used in this thesis showed remarkable results in both the light-driven production of H_2 as well as the reduction of CO_2, and this work represents one of the first successful attempts at the semi-artifical photosynthetic production of formate. Future projects investigating the efficiency of other semiconductors and the optimal conditions for scaling these systems up to industrial level will be key in order to tackle the continuous release of harmful greenhouses gases into the atmosphere and climate change.

6 References

1. Aziz M, Darmawan A, Juangsa FB. Hydrogen production from biomasses and wastes: A technological review. International Journal of Hydrogen Energy. 2021 Oct 1;46(68):33756–81.

2. Zohuri B. 2 - Nuclear fuel cycle and decommissioning. In: Khan SU-D, Nakhabov A, editors. Nuclear Reactor Technology Development and Utilization [Internet]. Woodhead Publishing; 2020 [cited 2021 Jul 21]. p. 61–120. (Woodhead Publishing Series in Energy). Available from: https://www.sciencedirect.com/science/article/pii/B9780128184837000020

3. Key World Energy Statistics 2020. :81.

4. Demirbaş A. Global Renewable Energy Resources. Energy Sources, Part A: Recovery, Utilization, and Environmental Effects. 2006 Jul 1;28(8):779–92.

5. Cherepovitsyn A, Chvileva T, Fedoseev S. Popularization of Carbon Capture and Storage Technology in Society: Principles and Methods. Int J Environ Res Public Health. 2020 Nov;17(22):8368.

6. bp Statistical Review of World Energy 2020. 2020;68.

7. 2050 long-term strategy [Internet]. [cited 2022 Mar 21]. Available from: https://ec.europa.eu/clima/eu-action/climate-strategies-targets/2050-long-term-strategy_en

8. The Paris Agreement | UNFCCC [Internet]. [cited 2022 Mar 2]. Available from: https://unfccc.int/process-and-meetings/the-paris-agreement/the-paris-agreement

9. Guan D, Meng J, Reiner DM, Zhang N, Shan Y, Mi Z, et al. Structural decline in China's CO2 emissions through transitions in industry and energy systems. Nature Geosci. 2018 Aug;11(8):551–5.

10. Pfeiffer A, Hepburn C, Vogt-Schilb A, Caldecott B. Committed emissions from existing and planned power plants and asset stranding required to meet the Paris Agreement. Environ Res Lett. 2018 May;13(5):054019.

11. Brancalion PHS, Holl KD. Guidance for successful tree planting initiatives. Journal of Applied Ecology. 2020;57(12):2349–61.

12. Holl KD, Brancalion PHS. Tree planting is not a simple solution. Science. 2020 May 8;368(6491):580–1.

13. Vercelli S, Anderlucci J, Memoli R, Battisti N, Mabon L, Lombardi S. Informing People about CCS: A Review of Social Research Studies. Energy Procedia. 2013 Jan 1;37:7464–73.

14. Al-Mamoori A, Krishnamurthy A, Rownaghi AA, Rezaei F. Carbon Capture and Utilization Update. Energy Technology. 2017;5(6):834–49.

15. Hoffert MI, Caldeira K, Benford G, Criswell DR, Green C, Herzog H, et al. Advanced Technology Paths to Global Climate Stability: Energy for a Greenhouse Planet. Science. 2002 Nov;298(5595):981–7.

16. Lewis NS, Nocera DG. Powering the planet: Chemical challenges in solar energy utilization. PNAS. 2006 Oct 24;103(43):15729–35.

17. Barber J. Photosynthetic energy conversion: natural and artificial. Chem Soc Rev. 2008 Dec 16;38(1):185–96.

18. Nayak PK, Mahesh S, Snaith HJ, Cahen D. Photovoltaic solar cell technologies: analysing the state of the art. Nature Reviews Materials. 2019 Mar 1;4:269–85.

19. Polman A, Knight M, Garnett EC, Ehrler B, Sinke WC. Photovoltaic materials: Present efficiencies and future challenges. Science. 2016 Apr 15;352(6283):aad4424.

20. Fang X, Kalathil S, Reisner E. Semi-biological approaches to solar-to-chemical conversion. Chem Soc Rev. 2020 Jul 21;49(14):4926–52.

21. Lewis NS, Crabtree G, Nozik AJ, Wasielewski MR, Alivisatos P, Kung H, et al. Basic Research Needs for Solar Energy Utilization. Report of the Basic Energy Sciences Workshop on Solar Energy Utilization, April 18-21, 2005 [Internet]. DOESC (USDOE Office of Science (SC)); 2005 Apr [cited 2022 Feb 24]. Available from: https://www.osti.gov/biblio/899136

22. Huynh WU, Dittmer JJ, Alivisatos AP. Hybrid Nanorod-Polymer Solar Cells. Science. 2002 Mar 29;295(5564):2425–7.

23. Grätzel M. Photoelectrochemical cells. In: Materials for Sustainable Energy [Internet]. Co-Published with Macmillan Publishers Ltd, UK; 2010 [cited 2022 Feb 24]. p. 26–32. Available from: https://www.worldscientific.com/doi/abs/10.1142/9789814317665_0003

24. Green MA, Emery K, King DL, Igari S, Warta W. SHORT COMMUNICATION: Solar cell efficiency tables (version 26). Prog Photovolt: Res Appl. 2005 Jan;13(1):49–54.

25. J. Frank A, Kopidakis N, Lagemaat J van de. Electrons in nanostructured TiO2 solar cells: transport, recombination and photovoltaic properties. Coordination Chemistry Reviews. 2004 Jul 1;248(13):1165–79.

26. Nowotny J, Sorrell CC, Sheppard LR, Bak T. Solar-hydrogen: Environmentally safe fuel for the future. International Journal of Hydrogen Energy. 2005 Apr 1;30(5):521–44.

27. Elam CC, Padró CEG, Sandrock G, Luzzi A, Lindblad P, Hagen EF. Realizing the hydrogen future: the International Energy Agency's efforts to advance hydrogen energy technologies. International Journal of Hydrogen Energy. 2003 Jun 1;28(6):601–7.

28. Bak T, Nowotny J, Rekas M, Sorrell CC. Photo-electrochemical hydrogen generation from water using solar energy. Materials-related aspects. International Journal of Hydrogen Energy. 2002 Oct 1;27(10):991–1022.

29. Ameta R, Solanki MS, Benjamin S, Ameta SC. Chapter 6 - Photocatalysis. In: Ameta SC, Ameta R, editors. Advanced Oxidation Processes for Waste Water Treatment [Internet]. Academic Press; 2018 [cited 2022 Mar 21]. p. 135–75. Available from: https://www.sciencedirect.com/science/article/pii/B9780128104996000061

30. Bao N, Shen L, Takata T, Domen K. Self-Templated Synthesis of Nanoporous CdS Nanostructures for Highly Efficient Photocatalytic Hydrogen Production under Visible Light. Chem Mater. 2008 Jan 1;20(1):110–7.

31. Yan H, Yang J, Ma G, Wu G, Zong X, Lei Z, et al. Visible-light-driven hydrogen production with extremely high quantum efficiency on Pt–PdS/CdS photocatalyst. Journal of Catalysis. 2009 Sep 10;266(2):165–8.

32. Silva CG, Bouizi Y, Fornés V, García H. Layered Double Hydroxides as Highly Efficient Photocatalysts for Visible Light Oxygen Generation from Water. J Am Chem Soc. 2009 Sep 30;131(38):13833–9.

33. Maeda K, Domen K. New Non-Oxide Photocatalysts Designed for Overall Water Splitting under Visible Light. J Phys Chem C. 2007 Jun 1;111(22):7851–61.

34. M. Navarro R, C. Sánchez-Sánchez M, C. Alvarez-Galvan M, del Valle F, G. Fierro JL. Hydrogen production from renewable sources: biomass and photocatalytic opportunities. Energy & Environmental Science. 2009;2(1):35–54.

35. Fujishima A, Honda K. Electrochemical Evidence for the Mechanism of the Primary Stage of Photosynthesis. BCSJ. 1971 Apr;44(4):1148–50.

36. Fujishima A, Honda K. Electrochemical Photolysis of Water at a Semiconductor Electrode. Nature. 1972 Jul;238(5358):37–8.

37. Ismail AA, Bahnemann DW. Photochemical splitting of water for hydrogen production by photocatalysis: A review. Solar Energy Materials and Solar Cells. 2014 Sep 1;128:85–101.

38. Tong H, Ouyang S, Bi Y, Umezawa N, Oshikiri M, Ye J. Nano-photocatalytic Materials: Possibilities and Challenges. Advanced Materials. 2012;24(2):229–51.

39. Chen X, Shen S, Guo L, Mao SS. Semiconductor-based Photocatalytic Hydrogen Generation. Chem Rev. 2010 Nov 10;110(11):6503–70.

40. Inoue T, Fujishima A, Konishi S, Honda K. Photoelectrocatalytic reduction of carbon dioxide in aqueous suspensions of semiconductor powders. Nature. 1979 Feb;277(5698):637–8.

41. Fu J, Jiang K, Qiu X, Yu J, Liu M. Product selectivity of photocatalytic CO2 reduction reactions. Materials Today. 2020 Jan 1;32:222–43.

42. Ran J, Jaroniec M, Qiao S-Z. Cocatalysts in Semiconductor-based Photocatalytic CO2 Reduction: Achievements, Challenges, and Opportunities. Advanced Materials. 2018;30(7):1704649.

43. Kovacs K, Maróti G, Rákhely G. A novel approach for biohydrogen production. International Journal of Hydrogen Energy. 2006 Sep 1;31:1460–8.

44. Vignais PM, Billoud B. Occurrence, Classification, and Biological Function of Hydrogenases: An Overview. Chem Rev. 2007 Oct 1;107(10):4206–72.

45. Lubitz W, Ogata H, Rüdiger O, Reijerse E. Hydrogenases. Chem Rev. 2014 Apr 23;114(8):4081–148.

46. Lubitz W, Tumas W. Hydrogen: An Overview. Chem Rev. 2007 Oct 1;107(10):3900–3.

47. Krasna AI. Hydrogenase: Properties and applications. Enzyme and Microbial Technology. 1979 Jul 1;1(3):165–72.

48. Baffert C, Kpebe A, Avilan L, Brugna M. Chapter Three - Hydrogenases and H2 metabolism in sulfate-reducing bacteria of the Desulfovibrio genus. In: Poole RK, editor. Advances in Microbial Physiology [Internet]. Academic Press; 2019 [cited 2021 Dec 14]. p. 143–89. (Advances in Microbial Physiology; vol. 74). Available from: https://www.sciencedirect.com/science/article/pii/S0065291119300098

49. Ntaikou I. 10 - Microbial production of hydrogen. In: Dutta S, Mustansar Hussain C, editors. Sustainable Fuel Technologies Handbook [Internet]. Academic Press; 2021 [cited 2022 Feb 25]. p. 315–37. Available from: https://www.sciencedirect.com/science/article/pii/B9780128229897000111

50. Hallenbeck PC, Benemann JR. Biological hydrogen production; fundamentals and limiting processes. International Journal of Hydrogen Energy. 2002 Nov 1;27(11):1185–93.

51. Benemann J. Hydrogen biotechnology: Progress and prospects. Nature Biotechnology. 1996;14(9):1101–3.

52. Kung Y, Drennan CL. A role for nickel–iron cofactors in biological carbon monoxide and carbon dioxide utilization. Current Opinion in Chemical Biology. 2011 Apr 1;15(2):276–83.

53. Alfano M, Cavazza C. The biologically mediated water–gas shift reaction: structure, function and biosynthesis of monofunctional [NiFe]-carbon monoxide dehydrogenases. Sustainable Energy Fuels. 2018 Jul 24;2(8):1653–70.

54. Kim D-H, Lee J-H, Kang S, Hallenbeck PC, Kim E-J, Lee JK, et al. Enhanced photo-fermentative H2 production using Rhodobacter sphaeroides by ethanol addition and analysis of soluble microbial products. Biotechnology for Biofuels. 2014 May 27;7(1):79.

55. Das D, Veziroğlu TN. Hydrogen production by biological processes: a survey of literature. International Journal of Hydrogen Energy. 2001 Jan 1;26(1):13–28.

56. Bryant DA, Frigaard N-U. Prokaryotic photosynthesis and phototrophy illuminated. Trends in Microbiology. 2006;14(11):488–96.

57. Hwang J-H, Kabra AN, Kim JR, Jeon B-H. Photoheterotrophic microalgal hydrogen production using acetate- and butyrate-rich wastewater effluent. Energy. 2014 Dec 15;78:887–94.

58. Branduardi P, Sauer M. Microbial carbon dioxide fixation: new tricks for an old game. FEMS Microbiology Letters. 2018 Feb 1;365(3):fnx269.

59. Sleep NH, Bird DK. Evolutionary ecology during the rise of dioxygen in the Earth's atmosphere. Philosophical Transactions of the Royal Society B: Biological Sciences. 2008 Aug 27;363(1504):2651–64.

60. Wong TS. Carbon Dioxide Capture and Utilization using Biological Systems: Opportunities and Challenges. J Bioprocess Biotech [Internet]. 2014 [cited 2022 Feb 28];04(03). Available from: https://www.omicsonline.org/open-access/carbon-dioxide-capture-and-utilization-using-biological-systems-opportunities-and-challenges-2155-9821.1000155.php?aid=25441

61. Ragsdale SW, Pierce E. Acetogenesis and the Wood–Ljungdahl pathway of CO2 fixation. Biochimica et Biophysica Acta (BBA) - Proteins and Proteomics. 2008 Dec 1;1784(12):1873–98.

62. Sahoo PC, Pant D, Kumar M, Puri SK, Ramakumar SSV. Material–Microbe Interfaces for Solar-Driven CO2 Bioelectrosynthesis. Trends in Biotechnology. 2020 Nov 1;38(11):1245–61.

63. Cestellos-Blanco S, Zhang H, Kim JM, Shen Y, Yang P. Photosynthetic semiconductor biohybrids for solar-driven biocatalysis. Nature Catalysis. 2020 Mar;3(3):245–55.

64. Müller V, Wiechmann A. Synthesis of Acetyl-CoA from Carbon Dioxide in Acetogenic Bacteria. In: Geiger O, editor. Biogenesis of Fatty Acids, Lipids and Membranes [Internet].

Cham: Springer International Publishing; 2017 [cited 2022 Mar 21]. p. 1–18. (Handbook of Hydrocarbon and Lipid Microbiology). Available from: https://doi.org/10.1007/978-3-319-43676-0_4-1

65. Sun Y, He J, Yang G, Sun G, Sage V. A Review of the Enhancement of Bio-Hydrogen Generation by Chemicals Addition. Catalysts. 2019 Apr;9(4):353.

66. Blankenship RE, Tiede DM, Barber J, Brudvig GW, Fleming G, Ghirardi M, et al. Comparing Photosynthetic and Photovoltaic Efficiencies and Recognizing the Potential for Improvement. Science. 2011 May 13;332(6031):805–9.

67. Meyer TJ. Chemical approaches to artificial photosynthesis. Acc Chem Res. 1989 May 1;22(5):163–70.

68. Appel AM, Bercaw JE, Bocarsly AB, Dobbek H, DuBois DL, Dupuis M, et al. Frontiers, Opportunities, and Challenges in Biochemical and Chemical Catalysis of CO2 Fixation. Chem Rev. 2013 Aug 14;113(8):6621–58.

69. Lovley DR. Electromicrobiology. Annu Rev Microbiol. 2012;66:391–409.

70. Sakimoto KK, Kornienko N, Cestellos-Blanco S, Lim J, Liu C, Yang P. Physical Biology of the Materials–Microorganism Interface. J Am Chem Soc. 2018 Feb 14;140(6):1978–85.

71. Yang N, Tian Y, Zhang M, Peng X, Li F, Li J, et al. Photocatalyst-enzyme hybrid systems for light-driven biotransformation. Biotechnology Advances. 2022 Jan 1;54:107808.

72. Brown KA, Harris DF, Wilker MB, Rasmussen A, Khadka N, Hamby H, et al. Light-driven dinitrogen reduction catalyzed by a CdS:nitrogenase MoFe protein biohybrid. Science. 2016 Apr 22;352(6284):448–50.

73. Vignais PM, Billoud B, Meyer J. Classification and phylogeny of hydrogenases1. FEMS Microbiology Reviews. 2001 Aug 1;25(4):455–501.

74. King PW. Designing interfaces of hydrogenase–nanomaterial hybrids for efficient solar conversion. Biochimica et Biophysica Acta (BBA) - Bioenergetics. 2013 Aug 1;1827(8):949–57.

75. Reisner E. Solar Hydrogen Evolution with Hydrogenases: From Natural to Hybrid Systems. European Journal of Inorganic Chemistry. 2011;2011(7):1005–16.

76. Reisner E, Powell DJ, Cavazza C, Fontecilla-Camps JC, Armstrong FA. Visible Light-Driven H2 Production by Hydrogenases Attached to Dye-Sensitized TiO2 Nanoparticles. J Am Chem Soc. 2009 Dec 30;131(51):18457–66.

77. Morra S, Valetti F, J. Sadeghi S, W. King P, Meyer T, Gilardi G. Direct electrochemistry of an [FeFe]-hydrogenase on a TiO 2 Electrode. Chemical Communications. 2011;47(38):10566–8.

78. Cuendet P, Rao KK, Grätzel M, Hall DO. Light induced H2 evolution in a hydrogenase-TiO2 particle system by direct electron transfer or via Rhodium complexes. Biochimie. 1986 Jan 1;68(1):217–21.

79. A. Caputo C, Wang L, Beranek R, Reisner E. Carbon nitride–TiO 2 hybrid modified with hydrogenase for visible light driven hydrogen production. Chemical Science. 2015;6(10):5690–4.

80. Holá K, Pavliuk MV, Németh B, Huang P, Zdražil L, Land H, et al. Carbon Dots and [FeFe] Hydrogenase Biohybrid Assemblies for Efficient Light-Driven Hydrogen Evolution. ACS Catal. 2020 Sep 4;10(17):9943–52.

81. Brown KA, Wilker MB, Boehm M, Dukovic G, King PW. Characterization of Photochemical Processes for H2 Production by CdS Nanorod–[FeFe] Hydrogenase Complexes. J Am Chem Soc. 2012 Mar 28;134(12):5627–36.

82. Hutton GAM, Reuillard B, Martindale BCM, Caputo CA, Lockwood CWJ, Butt JN, et al. Carbon Dots as Versatile Photosensitizers for Solar-Driven Catalysis with Redox Enzymes. J Am Chem Soc. 2016 Dec 28;138(51):16722–30.

83. Oliveira AR, Mota C, Mourato C, Domingos RM, Santos MFA, Gesto D, et al. Toward the Mechanistic Understanding of Enzymatic CO2 Reduction. ACS Catal. 2020 Mar 20;10(6):3844–56.

84. Boddien A, Mellmann D, Gärtner F, Jackstell R, Junge H, Dyson PJ, et al. Efficient Dehydrogenation of Formic Acid Using an Iron Catalyst. Science. 2011 Sep 23;333(6050):1733–6.

85. Amao Y, Shuto N. Formate dehydrogenase–viologen-immobilized electrode for CO2 conversion, for development of an artificial photosynthesis system. Res Chem Intermed. 2014 Nov 1;40(9):3267–76.

86. Miller M, Robinson WE, Oliveira AR, Heidary N, Kornienko N, Warnan J, et al. Interfacing Formate Dehydrogenase with Metal Oxides for the Reversible Electrocatalysis and Solar-Driven Reduction of Carbon Dioxide. Angewandte Chemie International Edition. 2019;58(14):4601–5.

87. Toyodome T, Amao Y, Higashi M. Photoelectrochemical reduction of CO 2 to formate over a hybrid system of CuInS 2 photocathode and formate dehydrogenase under visible-light irradiation. New Journal of Chemistry. 2021;45(32):14803–7.

88. Hernández-Ibáñez N, Gomis-Berenguer A, Montiel V, Ania CO, Iniesta J. Fabrication of a biocathode for formic acid production upon the immobilization of formate dehydrogenase from Candida boidinii on a nanoporous carbon. Chemosphere. 2022 Mar 1;291:133117.

89. Miyatani R, Amao Y. Photochemical synthesis of formic acid from CO2 with formate dehydrogenase and water-soluble zinc porphyrin. Journal of Molecular Catalysis B: Enzymatic. 2004 Feb 2;27(2):121–5.

90. Litman ZC, Wang Y, Zhao H, Hartwig JF. Cooperative asymmetric reactions combining photocatalysis and enzymatic catalysis. Nature. 2018 Aug;560(7718):355–9.

91. Yadav RK, Baeg J-O, Oh GH, Park N-J, Kong K, Kim J, et al. A Photocatalyst–Enzyme Coupled Artificial Photosynthesis System for Solar Energy in Production of Formic Acid from CO2. J Am Chem Soc. 2012 Jul 18;134(28):11455–61.

92. Kornienko N, Zhang JZ, Sakimoto KK, Yang P, Reisner E. Interfacing nature's catalytic machinery with synthetic materials for semi-artificial photosynthesis. Nature Nanotechnology. 2018 Oct;13(10):890–9.

93. Sarma AK, Vatsyayan P, Goswami P, Minteer SD. Recent advances in material science for developing enzyme electrodes. Biosens Bioelectron. 2009 Apr 15;24(8):2313–22.

94. Liu C, Gallagher JJ, Sakimoto KK, Nichols EM, Chang CJ, Chang MCY, et al. Nanowire–Bacteria Hybrids for Unassisted Solar Carbon Dioxide Fixation to Value-Added Chemicals. Nano Lett. 2015 May 13;15(5):3634–9.

95. Honda Y, Hagiwara H, Ida S, Ishihara T. Application to Photocatalytic H2 Production of a Whole-Cell Reaction by Recombinant Escherichia coli Cells Expressing [FeFe]-Hydrogenase and Maturases Genes. Angewandte Chemie International Edition. 2016;55(28):8045–8.

96. Honda Y, Watanabe M, Hagiwara H, Ida S, Ishihara T. Inorganic/whole-cell biohybrid photocatalyst for highly efficient hydrogen production from water. Applied Catalysis B: Environmental. 2017 Aug 5;210:400–6.

97. Rowe SF, Le Gall G, Ainsworth EV, Davies JA, Lockwood CWJ, Shi L, et al. Light-Driven H2 Evolution and C═C or C═O Bond Hydrogenation by Shewanella oneidensis: A Versatile Strategy for Photocatalysis by Nonphotosynthetic Microorganisms. ACS Catal. 2017 Nov 3;7(11):7558–66.

98. Quintana N, Van der Kooy F, Van de Rhee MD, Voshol GP, Verpoorte R. Renewable energy from Cyanobacteria: energy production optimization by metabolic pathway engineering. Appl Microbiol Biotechnol. 2011;91(3):471–90.

99. Fast A, Papoutsakis E. Stoichiometric and energetic analyses of non-photosynthetic CO2-fixation pathways to support synthetic biology strategies for production of fuels and chemicals. Current Opinion in Chemical Engineering. 2012 Nov 1;1:380–95.

100. Sweeney RY, Mao C, Gao X, Burt JL, Belcher AM, Georgiou G, et al. Bacterial biosynthesis of cadmium sulfide nanocrystals. Chem Biol. 2004 Nov;11(11):1553–9.

101. Cheng L, Xiang Q, Liao Y, Zhang H. CdS-Based photocatalysts. Energy and Environmental Science. 2018;11(6):1362–91.

102. Oguri T, Schneider B, Reitzer L. Cysteine Catabolism and Cysteine Desulfhydrase (CdsH/STM0458) in Salmonella enterica Serovar Typhimurium. J Bacteriol. 2012 Aug;194(16):4366–76.

103. Drake HL, Daniel SL. Physiology of the thermophilic acetogen Moorella thermoacetica. Res Microbiol. 2004 Dec;155(10):869–83.

104. Sakimoto K, Wong A, Yang P. Self-photosensitization of nonphotosynthetic bacteria for solar-to-chemical production. Science. 2016 Jan 1;351:74–7.

105. Ye J, Yu J, Zhang Y, Chen M, Liu X, Zhou S, et al. Light-driven carbon dioxide reduction to methane by Methanosarcina barkeri-CdS biohybrid. 2019;

106. Wang B, Zeng C, Chu KH, Wu D, Yip HY, Ye L, et al. Enhanced Biological Hydrogen Production from Escherichia coli with Surface Precipitated Cadmium Sulfide Nanoparticles. Advanced Energy Materials. 2017;7(20):1700611.

107. Jiang Z, Wang B, Yu JC, Wang J, An T, Zhao H, et al. AglnS2/In2S3 heterostructure sensitization of Escherichia coli for sustainable hydrogen production. Nano Energy. 2018 Apr 1;46:234–40.

108. Wei W, Sun P, Li Z, Song K, Su W, Wang B, et al. A surface-display biohybrid approach to light-driven hydrogen production in air. Sci Adv. 2018 Feb;4(2):eaap9253.

109. Silhavy TJ, Kahne D, Walker S. The bacterial cell envelope. Cold Spring Harb Perspect Biol. 2010 May;2(5):a000414.

110. Zhang H, Liu H, Tian Z, Lu D, Yu Y, Cestellos-Blanco S, et al. Bacteria photosensitized by intracellular gold nanoclusters for solar fuel production. Nature Nanotechnology. 2018 Oct;13(10):900–5.

111. Deplanche K, Macaskie LE. Biorecovery of gold by Escherichia coli and Desulfovibrio desulfuricans. Biotechnology and Bioengineering. 2008;99(5):1055–64.

112. Ahmed E, Kalathil S, Shi L, Alharbi O, Wang P. Synthesis of ultra-small platinum, palladium and gold nanoparticles by Shewanella loihica PV-4 electrochemically active biofilms and their enhanced catalytic activities. Journal of Saudi Chemical Society. 2018 Dec 1;22(8):919–29.

113. Luo B, Wang Y-Z, Li D, Shen H, Xu L-X, Fang Z, et al. A Periplasmic Photosensitized Biohybrid System for Solar Hydrogen Production. Advanced Energy Materials. 2021;11(19):2100256.

114. Martins M, Toste C, Pereira IAC. Enhanced Light-Driven Hydrogen Production by Self-Photosensitized Biohybrid Systems. Angewandte Chemie International Edition. 2021;60(16):9055–62.

115. da Silva SM, Voordouw J, Leitão C, Martins M, Voordouw G, Pereira IACY 2013. Function of formate dehydrogenases in Desulfovibrio vulgaris Hildenborough energy metabolism. Microbiology. 159(Pt_8):1760–9.

116. Caffrey SM, Park H-S, Voordouw JK, He Z, Zhou J, Voordouw G. Function of Periplasmic Hydrogenases in the Sulfate-Reducing Bacterium Desulfovibrio vulgaris Hildenborough. J Bacteriol. 2007 Sep;189(17):6159–67.

117. Martins M, Mourato C, Sanches S, Noronha JP, Crespo MTB, Pereira IAC. Biogenic platinum and palladium nanoparticles as new catalysts for the removal of pharmaceutical compounds. Water Research. 2017 Jan 1;108:160–8.

118. Hosseini SMR, Nasiri Sarvi M. Recent achievements in the microbial synthesis of semiconductor metal sulfide nanoparticles. Materials Science in Semiconductor Processing. 2015 Dec 1;40:293–301.

119. Photochemical Purification of Water and Air: Advanced Oxidation Processes (AOPs) - Principles, Reaction Mechanisms, Reactor Concepts | Wiley [Internet]. Wiley.com. [cited 2022 Jan 18]. Available from: https://www.wiley.com/en-us/Photochemical+Purification+of+Water+and+Air%3A+Advanced+Oxidation+Processes+%28AOPs%29+Principles%2C+Reaction+Mechanisms%2C+Reactor+Concepts-p-9783527610891

120. Mourato C, Martins M, da Silva SM, Pereira IAC. A continuous system for biocatalytic hydrogenation of CO2 to formate. Bioresour Technol. 2017 Jul;235:149–56.

121. Dong G, Wang H, Yan Z, Zhang J, Ji X, Lin M, et al. Cadmium sulfide nanoparticles-assisted intimate coupling of microbial and photoelectrochemical processes: Mechanisms and environmental applications. Sci Total Environ. 2020 Oct 20;740:140080.

122. Yang J, Wang D, Han H, Li C. Roles of Cocatalysts in Photocatalysis and Photoelectrocatalysis. Acc Chem Res. 2013 Aug 20;46(8):1900–9.

123. Mills A. LS. Platinum and palladium in semiconductor photocatalytic systems. Platinum metals review. 2003;47(2):61–72.

124. Learn How Platinum and Palladium Bullion Compare | Provident [Internet]. Provident Metals. 2019 [cited 2022 Mar 22]. Available from: https://www.providentmetals.com/knowledge-center/precious-metals-resources/comparing-platinum-palladium.html

125. Yuan S, Chen M, Mao X, Alshawabkeh AN. Effects of Reduced Sulfur Compounds on Pd-catalytic Hydrodechlorination of TCE in Groundwater by Cathodic H2 under Electrochemically-induced Oxidizing Conditions. Environ Sci Technol. 2013 Sep 17;47(18):10502–9.

126. Zhang L, Chang Q, Chen H, Shao M. Recent advances in palladium-based electrocatalysts for fuel cell reactions and hydrogen evolution reaction. Nano Energy. 2016 Nov 1;29:198–219.

127. Chen X, Shangguan W. Hydrogen production from water splitting on CdS-based photocatalysts using solar light. Front Energy. 2013 Mar 1;7(1):111–8.

128. Cao S, Wang C-J, Fu W-F, Chen Y. Metal Phosphides as Co-Catalysts for Photocatalytic and Photoelectrocatalytic Water Splitting. ChemSusChem. 2017;10(22):4306–23.

129. Zong X, Yan H, Wu G, Ma G, Wen F, Wang L, et al. Enhancement of Photocatalytic H2 Evolution on CdS by Loading MoS2 as Cocatalyst under Visible Light Irradiation. J Am Chem Soc. 2008 Jun 1;130(23):7176–7.

130. Brown KA, King PW. Coupling biology to synthetic nanomaterials for semi-artificial photosynthesis. Photosynth Res. 2020 Feb;143(2):193–203.

131. Ye J, Ren G, Kang L, Zhang Y, Liu X, Zhou S, et al. Efficient Photoelectron Capture by Ni Decoration in Methanosarcina barkeri-CdS Biohybrids for Enhanced Photocatalytic CO2-to-CH4 Conversion. iScience. 2020 Jul 24;23(7):101287.

132. Zhong W, Tu W, Feng S, Xu A. Photocatalytic H2 evolution on CdS nanoparticles by loading FeSe nanorods as co-catalyst under visible light irradiation. Journal of Alloys and Compounds. 2019 Jan 25;772:669–74.

133. Light-driven carbon dioxide reduction to methane by Methanosarcina barkeri-CdS biohybrid - Appl. Catal. B Environ. - X-MOL [Internet]. [cited 2020 Sep 25]. Available from: https://www.x-mol.com/paper/5757007?recommendNews=461909

134. Zhang ZJ, Zhang J, Xue QJ. Synthesis and Characterization of a Molybdenum Disulfide Nanocluster. The Journal of Physical Chemistry. 1994 Dec;98(49):12973–7.

135. Kumar M, Sahoo PC, Srikanth S, Bagai R, Puri SK, Ramakumar SSV. Photosensitization of electro-active microbes for solar assisted carbon dioxide transformation. Bioresource Technology. 2019 Jan 1;272:300–7.

136. Capeness MJ, Edmundson MC, Horsfall LE. Nickel and platinum group metal nanoparticle production by Desulfovibrio alaskensis G20. New Biotechnology. 2015 Dec 25;32(6):727–31.

137. Wu X, Zhao F, Rahunen N, Varcoe JR, Avignone-Rossa C, Thumser AE, et al. A Role for Microbial Palladium Nanoparticles in Extracellular Electron Transfer. Angewandte Chemie International Edition. 2011;50(2):427–30.

138. Saravanan A, Kumar PS, Karishma S, Vo D-VN, Jeevanantham S, Yaashikaa PR, et al. A review on biosynthesis of metal nanoparticles and its environmental applications. Chemosphere. 2021 Feb 1;264:128580.

139. Fud R, Voordouw G 1997. Targeted gene-replacement mutagenesis of dcrA, encoding an oxygen sensor of the sulfate-reducing bacterium Desulfovibrio vulgaris Hildenborough. Microbiology. 143(6):1815–26.

140. Keller KL, Bender KS, Wall JD. Development of a Markerless Genetic Exchange System for Desulfovibrio vulgaris Hildenborough and Its Use in Generating a Strain with Increased Transformation Efficiency. Applied and Environmental Microbiology. 2009 Dec 15;75(24):7682–91.

141. Morais-Silva FO, Rezende AM, Pimentel C, Santos CI, Clemente C, Varela–Raposo A, et al. Genome sequence of the model sulfate reducer Desulfovibrio gigas: a comparative analysis within the Desulfovibrio genus. Microbiologyopen. 2014 Aug;3(4):513–30.

142. Pereira IAC, Ramos AR, Grein F, Marques MC, da Silva SM, Venceslau SS. A comparative genomic analysis of energy metabolism in sulfate reducing bacteria and archaea. Front Microbiol. 2011;2:69.

143. Valente FMA, Almeida CC, Pacheco I, Carita J, Saraiva LM, Pereira IAC. Selenium Is Involved in Regulation of Periplasmic Hydrogenase Gene Expression in Desulfovibrio vulgaris Hildenborough. Journal of Bacteriology. 2006 May 1;188(9):3228–35.

144. Silva SM da, Pimentel C, Valente FMA, Rodrigues-Pousada C, Pereira IAC. Tungsten and Molybdenum Regulation of Formate Dehydrogenase Expression in Desulfovibrio vulgaris Hildenborough. Journal of Bacteriology [Internet]. 2011 Apr 15 [cited 2022 Feb 2]; Available from: https://journals.asm.org/doi/abs/10.1128/JB.00042-11

145. Chen H, Ma X, Fan D, Luo Y, Gao P, Yang C. Influence of L-Cysteine Concentration on Oxidation-reduction Potential and Biohydrogen Production. Chinese Journal of Chemical Engineering. 2010 Aug 1;18(4):681–6.